

# Experimental Constraints on the Origin of the 1991 Pinatubo Dacite

GAËLLE PROUTEAU<sup>1</sup> and BRUNO SCAILLET<sup>2</sup>

<sup>1</sup> UMR 6538, UNIVERSITÉ DE BRETAGNE OCCIDENTALE, 6 AVENUE LE GORGEU, BP 29285, BREST, FRANCE

<sup>2</sup> INSTITUT DES SCIENCES DE LA TERRE D'ORLÉANS, CNRS, 1A RUE DE LA FÉROLLERIE, 45071 ORLÉANS CEDEX 2, FRANCE

RECEIVED JULY 18, 2002; ACCEPTED JUNE 5, 2003

## ABSTRACT

Crystallization (dacite) and interaction (dacite–peridotite) experiments have been performed on the 1991 Pinatubo dacite (Luzon Island, Philippines) to constrain its petrogenesis. In the dacite–H<sub>2</sub>O system at 960 MPa, magnetite and either clinopyroxene (low H<sub>2</sub>O) or amphibole (high H<sub>2</sub>O) are the liquidus phases. No garnet is observed at this pressure. Dacite–peridotite interaction at 920 MPa produces massive orthopyroxene crystallization, in addition to amphibole ± phlogopite. Amphibole crystallizing in dacite at 960 MPa has the same composition as the aluminium-rich hornblende preserved in the cores of amphibole phenocrysts in the 1991 dacite, suggesting a high-pressure stage of dacite crystallization with high melt H<sub>2</sub>O contents (>10 wt %) at relatively low temperature (<950°C). The compositions of plagioclase, amphibole and melt inclusion suggest that the Pinatubo dacite was water-rich, oxidized and not much hotter than 900°C, when emplaced into the shallow magma reservoir in which most phenocrysts precipitated before the onset of the 1991 eruption. The LREE-enriched REE pattern of the whole-rock dacite demands garnet somewhere during its petrogenesis, which in turn suggests high-pressure derivation. Partial melting of subducted oceanic crust yields melts unlike the Pinatubo dacite. Interaction of these slab melts with sub-arc peridotite is unable to produce a Pinatubo type of dacite, nor is a direct mantle origin conceivable on the basis of our peridotite–dacite interaction experimental results. Dehydration melting of underplated basalts requires unrealistically high temperatures and does not yield dacite with the low FeO/MgO, and high H<sub>2</sub>O, Ni and Cr contents typical of the Pinatubo dacite. The most plausible origin of the Pinatubo dacite is via high-pressure fractionation of a hydrous, oxidized, primitive basalt that crystallized amphibole and garnet upon cooling. Dacite melts produced in this way were directly expelled from the uppermost mantle or lower crust to shallow-level reservoirs from which they erupted occasionally. Magmas such as the Pinatubo dacite may provide evidence for the existence of particularly H<sub>2</sub>O-rich conditions in the sub-arc mantle wedge rather than the melting of the young, hot subducting oceanic plate.

KEY WORDS: *Pinatubo dacite; slab melt; experimental petrology; arc magmas*

# INTRODUCTION

Despite numerous studies, there is at present no consensus regarding the origin of siliceous low-K magmas in island and continental-margin arcs. Petrogenetic models for the origin of felsic arc magmas fall into two broad categories: (1) a common opinion is that these magmas are derived from low-K basaltic parents by fractional crystallization or AFC processes (assimilation plus fractional crystallization) (e.g. Arth *et al.*, 1978; Tomblin, 1979; Barnes *et al.*, 1992; Singer *et al.*, 1992); (2) a second category of models proposes that these magmas are generated by partial melting of crustal protoliths (e.g. Gill & Stork, 1979; Smith & Leeman, 1987; Wareham *et al.*, 1997; Costa & Singer, 2002), including metamorphosed mafic igneous rocks that form a dominant constituent of the lower arc crust (e.g. Beard & Day, 1988). Following Coats (1962), it has also been suggested that partial melting of the basaltic portion of the subducted oceanic lithosphere may contribute to the petrogenesis of silicic magmas (e.g. Green & Ringwood, 1968; Kay, 1978; Kay *et al.*, 1993; Drummond *et al.*, 1996). Defant & Drummond (1990) and Drummond & Defant (1990) have proposed a slab melt origin for some high Al<sub>2</sub>O<sub>3</sub> Cenozoic trondhjemite–tonalite–dacite (TTD) magmas also referred to as adakites. Adakites have distinctive geochemical signatures; in particular, strongly fractionated rare earth element (REE) patterns, with La typically ranging from 40 to 150 ppm and very low heavy REE (HREE) contents (Yb <1.8 ppm; Y <18 ppm). There is a general consensus that the presence of garnet is required at some stage in the petrogenesis of adakites, either as a residual phase in the source or as an early crystallizing phenocryst phase, to account for their steep REE patterns. Consequently, many researchers have proposed a deep-seated origin for adakite-like magmas. However, whether the source is in the lower arc crust (e.g. Smith & Leeman, 1987; Petford & Atherton, 1996) or the subducted oceanic crust (e.g. Drummond & Defant, 1990; Stern & Kilian, 1996; Bourdon *et al.*, 2002) is still a matter of debate.

In this paper we present the results of an experimental study performed on the phenocryst-rich Mt Pinatubo dacite erupted on June 15, 1991. This dacite exhibits all the mineralogical and chemical features diagnostic of Cenozoic adakites (e.g. Bernard *et al.*, 1996). We provide experimental results for the dacite–H<sub>2</sub>O system at 400 and 960 MPa that build upon previous experimental work carried out on the Pinatubo dacite at 220 MPa (Rutherford & Devine, 1996; Scaillet & Evans, 1999). By working out the phase relations and mineral composition of the dacite at several pressures we can constrain the magmatic evolution of adakite-like magmas. Such an inverse experimental strategy has been already applied to some Archaean TTD (Van der Laan & Wyllie, 1992) but never to Cenozoic examples, apart from the preliminary results of Prouteau *et al.* (1999). In addition, we have performed experiments to evaluate the interaction between hydrous dacite and peridotite minerals at 920 MPa, temperatures between 950 and 1000°C, and under oxidizing conditions, in an effort to evaluate the role of melt–rock reaction in the mantle on dacite–adakite petrogenesis.

# GEOLOGICAL SETTING AND ERUPTIVE HISTORY OF MOUNT PINATUBO

Pinatubo is located in the west of the central part of Luzon Island, Philippines. It is part of the Bataan volcanic segment of the Taiwan–Luzon arc (Defant *et al.*, 1989, 1991). The currently active volcanic arc is related to the east-dipping Manila subduction zone and has been active since the late Miocene, although most volcanism occurred in the Quaternary and late Pliocene (Richard *et al.*, 1986). The oceanic crust entering the trench is part of the South China Sea oceanic basin, which opened during the Miocene (Briais *et al.*, 1993). The age of oceanic crust subducting along the Pinatubo transect can be estimated from palaeomagnetic constraints to be 10–15 Ma (Briais *et al.*, 1993). Geophysical evidence shows that the Benioff zone lies ~100 km beneath the volcano (Cardwell *et al.*, 1980; de Boer *et al.*, 1980). Mount Pinatubo is a moderate-sized edifice whose height prior to eruption was 1745 m above sea level, subsequently being reduced to 1450 m after the 1991 explosive events. Exploratory geothermal drill cores have shown that the volcano lies on ~2–4 km andesite–dacite deposits (Delfin *et al.*, 1996). This volcanic–sedimentary pile is probably underlain by the eastward and downward extension of the Eocene Zambales ophiolite complex. Seismic monitoring during the 1991 eruptions suggested the existence of a magma body at depth of at least 40–90 km<sup>3</sup>, but perhaps as great as 140 km<sup>3</sup> (Mori *et al.*, 1996). This would make the Pinatubo area one of the largest active magmatic areas known so far in arc regions worldwide.

The eruptive history of Pinatubo has been divided into an ancestral (1 Ma–35 ka BP) and a modern (<35 ka) period (Delfin, 1984; Newhall *et al.*, 1996). Available radiometric constraints suggest that Pinatubo has experienced at least six major eruptions over the last 35 kyr, and that the last eruption before the 1991 eruptive cycle occurred some 500–600 years ago (Newhall *et al.*, 1996). The volume and magnitude of each eruption, as well as the repose time between eruptions, seem to decrease with time, from 20–25 km<sup>3</sup> (dense rock equivalent, DRE) for the first eruption of the modern period to about 5 km<sup>3</sup> DRE for the last two events (500–600 years ago and the 1991 events). The deposits of each eruption preserve evidence that each eruptive cycle followed a pattern similar to that observed during the 1991 events: the main erupted component was a cummingtonite-bearing dacite (SiO<sub>2</sub> 62–67 wt %), together with a volumetrically minor mafic hybrid magma, generally andesitic, that formed following the injection of a mafic magma into the relatively cold and gas-saturated silicic magma reservoir. Although injection of mafic magma seems to happen frequently and may even be the ultimate trigger of each explosive event (Pallister *et al.*, 1996), the composition of the bulk of erupted magma has remained remarkably constant over the past 35 kyr (Newhall *et al.*, 1996). As stressed by Newhall *et al.* (1996), the systematic occurrence of cummingtonite in the dacites also indicates that the  $P$ – $T$ – $f_{\text{O}_2}$ – $f_{\text{H}_2\text{O}}$  storage conditions of the erupted magmas were similar to those of the 1991 dacite; that is, pressure lower than 300 MPa, temperature below 780°C and water-rich conditions (Rutherford & Devine, 1996; Scaillet & Evans, 1999).

## THE 1991 PINATUBO DACITE

The Pinatubo dacite fulfils the compositional criteria required to classify it as an adakite (Table 1): it has a high  $\text{Al}_2\text{O}_3$  content (16.5 wt %) and  $\text{MgO}/(\text{FeO} + \text{MgO})$  ratio; low Y (<15 ppm) and Yb; high Sr (500–600 ppm) and Sr/Y (>35); high La/Yb; and lacks an Eu anomaly. The trace element characteristics suggest both the presence of garnet and absence of plagioclase in the source region (Defant & Drummond, 1990). Its Nd–Sr isotopic composition is compatible with derivation from a basaltic protolith (Bernard *et al.*, 1996). The high MgO content of adakites, together with elevated Ni and Cr values relative to typical calc-alkaline dacites, is usually interpreted to reflect interaction with the mantle wedge during magma uprise (e.g. Kay *et al.*, 1993; Sen & Dunn, 1994a, 1994b). The detection in two samples of phenocryst-rich pumices of high contents of the cosmogenic nuclide  $^{10}\text{Be}$  provides evidence for a sedimentary component in the petrogenesis of the dacite, presumably recycled through the subduction zone system (Bernard *et al.*, 1996).

The petrology of the eruptive products has been extensively described in previous studies (e.g. Bernard *et al.*, 1996; Fournelle *et al.*, 1996; Hattori, 1996; Hattori & Sato, 1996; Luhr & Melson, 1996; Pallister *et al.*, 1996; Rutherford & Devine, 1996) and only the salient features are reviewed here. Phenocryst-rich dacite pumices from the paroxysmal 1991 eruption contain ~50% (by volume) phenocrysts, mainly plagioclase (~30%) and hornblende (~10–15%) with cummingtonite overgrowths. Smaller amounts of biotite, quartz, ilmenite, magnetite, apatite, sulphides and anhydrite are also present. This phenocryst assemblage is typical of that of high-Al Cenozoic adakites, as defined by Drummond & Defant (1990), and is notable by the absence of pyroxene as a phenocryst or in the groundmass. Plagioclase phenocrysts are concentrically and variably zoned in the range  $\text{An}_{66-27}$  (Luhr & Melson, 1996; Pallister *et al.*, 1996; Rutherford & Devine, 1996), but compositions up to  $\text{An}_{80}$  have been reported by Hattori & Sato (1996). Rim compositions average  $\text{An}_{41}$ , but may be as low as  $\text{An}_{27}$  (Pallister *et al.*, 1996). Plagioclase and quartz phenocrysts contain abundant homogeneous glass inclusions with up to 6.4 wt %  $\text{H}_2\text{O}$  (Westrich & Gerlach, 1992; Rutherford & Devine, 1996). When normalized to an anhydrous basis, the glass inclusions have a high-silica rhyolite composition. They are similar to the matrix glass of the dacite, indicating a comagmatic origin and suggesting that post-entrapment crystallization was minimal (e.g. Gerlach *et al.*, 1996). Hornblende forms pleochroic green to light brown euhedral or broken phenocrysts. Euhedral phenocrysts are often rimmed by a 10–50  $\mu\text{m}$  thick colourless cummingtonite overgrowth. Apart from these overgrowths, the composition of hornblende is variable and two populations can be distinguished: the first type is a low- $\text{Al}_2\text{O}_3$  amphibole with weak chemical zonation (e.g. Rutherford & Devine, 1996), which forms the dominant type of hornblende phenocryst; it has an average  $\text{Al}_2\text{O}_3$  content of  $7.9 \pm 0.8$  wt % (Rutherford & Devine, 1996), although  $\text{Al}_2\text{O}_3$  contents as low as 5 wt % have been reported (Scaillet & Evans, 1999). This amphibole is demonstrably in equilibrium with the residual melt (Rutherford & Devine, 1996; Scaillet & Evans, 1999). The second type of hornblende corresponds to occasional cores that have  $\text{Al}_2\text{O}_3$  contents as high as 12.6 wt %, correlated with higher alkali and  $\text{TiO}_2$  contents (Bernard *et al.*, 1996; Fournelle *et al.*, 1996; Imai *et al.*, 1996; this study, see below). In the two types of hornblende the Mg number [ $\text{Mg}/(\text{Mg} + \text{Fe}_{\text{tot}})$ ] is high but is variable, ranging from 69 to 62, and there is no correlation between Mg number and  $\text{Al}_2\text{O}_3$  content (see below).

The phase relationships of the 1991 Pinatubo dacite have been investigated in detail at 220 MPa, i.e. the inferred pressure of phenocryst–melt pre-eruption equilibration, by Rutherford & Devine (1996) and Scaillet & Evans (1999). Phase equilibria at this pressure reproduce the

phenocryst assemblage of the magma at temperatures  $<780^{\circ}\text{C}$  and under water-rich conditions ( $\text{H}_2\text{O}_{\text{melt}} > 6 \text{ wt } \%$ ). Comparison between natural and experimental oxides indicates that magmatic  $f_{\text{O}_2}$  was in the range  $\text{NNO} + 1.5$  to  $\text{NNO} + 1.7$  (where NNO is the nickel–nickel oxide buffer) prior to eruption (Evans & Scaillet, 1997; Scaillet & Evans, 1999). The composition of plagioclase implies crystallization close to or at  $\text{H}_2\text{O}$ -saturation ( $\sim 7 \text{ wt } \%$  at this pressure) within the temperature range  $750\text{--}900^{\circ}\text{C}$  in an upper-crustal magma chamber. So far, all petrological studies have shown that the vast majority of plagioclase compositions range between  $\text{An}_{27}$  and  $\text{An}_{80}$ . However, plagioclase more calcic than  $\text{An}_{60}$  is exceedingly rare and has been reported only by Hattori & Sato (1996). According to published analyses, we estimate that the proportion of strongly calcic plagioclase does not exceed 1–3% of the plagioclase phenocrysts. Apart from the An-rich plagioclase and  $\text{Al}_2\text{O}_3$ -rich cores in hornblende, the experiments at 220 MPa reproduce all the mineral characteristics (mineral proportions and compositions) of the Pinatubo dacite, indicating that the vast majority of the phenocrysts are likely to have crystallized in the upper storage chamber. Thus, either the magma was in a nearly molten state when injected in the upper-crustal reservoir or any xenocrysts or mafic magma injected in the reservoir equilibrated with the host dacite.

## ROLE OF BASALT IN DACITE PETROGENESIS

The compositional similarity of the dacite magmas erupted over time at Pinatubo implies that either any recharge event involved a magma of dacite composition or the amount of mafic magma injected was too small to significantly affect the bulk composition of the resident magma over time (at least of that portion being erupted following injection). Similarly, the remarkable constancy of pre-eruptive conditions suggests that the buffering capacity of the dacite pluton against external factors such as mafic injections has been sufficiently large to avoid extreme and long-lasting thermal excursions over the last 35 kyr, perhaps as a result of the large size of the chamber compared with that of the many mafic magma inputs; yet the complex zoning patterns displayed by plagioclase phenocrysts (Hattori & Sato, 1996; Luhr & Melson, 1996) suggest a complex history of crystallization in response to repeated replenishment of the upper chamber and mixing of discrete magma batches and/or to the changing fluid dynamics of the magma in the reservoir before eruption (Hattori & Sato, 1996). However, as shown by Bernard *et al.* (1996) and Hattori & Sato (1996), plagioclase compositions define a single trend in an An–Or plot. This trend has been reproduced experimentally by Scaillet & Evans (1999), but under  $\text{H}_2\text{O}$ -saturated conditions only, in the temperature range  $760\text{--}900^{\circ}\text{C}$ . Thus, crystallization of the dacite under these conditions can produce the observed spread in plagioclase composition between  $\text{An}_{27}$  and  $\text{An}_{60}$ , and there is no need to call upon a mafic magma to explain the zoning pattern. This again suggests that each newly injected magma had a composition broadly similar to the resident one, i.e. it was a dacite magma close to  $\text{H}_2\text{O}$ -saturation, to maintain the Ca/Na and K/Na plagioclase–melt partitioning constant. Injection of mafic magma in significant proportion will make it difficult to maintain such a relationship: if a significant part of plagioclase phenocrysts had crystallized from a melt composition significantly different from dacite, then this should be reflected by a scatter of plagioclase compositions in an An–Or plot, which is not observed. Therefore, had the Pinatubo reservoir been fed in the remote past by a more mafic magma, then most of the mineralogical evidence of this event has been erased, either via chemical diffusion or by xenocryst dissolution, by the time the 1991 eruptions started.

The fact that there is no evidence in the eruptive products of any significant thermal or compositional zonation being developed or established in the reservoir prior to eruption (e.g. Pallister *et al.*, 1996), suggests also that, if the dacite magma is derived from basalt or andesite fractionation, then such a process must largely operate at levels significantly deeper than the reservoir tapped during the recent period. Given the size of the cooling pluton and that ~40–50 wt % of fractional crystallization of an hydrous basalt is required to generate residual hydrous dacitic liquids (Pichavant *et al.*, 2002a), this would imply the existence of a very large parental magma body, of about the size of the upper dacite pluton, at a depth equivalent to a pressure of at least 400–500 MPa. The analysis of the present-day seismic activity reveals the existence of a reservoir of at least 40–90 km<sup>3</sup>, but the original volume of dacite emplaced may have been larger given that some of it has frozen, possibly of the order of 200 km<sup>3</sup>. Considering that the volume of erupted dacite over the last 35 kyr amounts to >50 km<sup>3</sup> (Newhall *et al.*, 1996), this is viewed as a conservative estimate. A basalt fractionation model thus requires the production of voluminous amounts of basaltic magma, in contrast to their near total absence in the eruptive products of Mount Pinatubo, apart from those co-erupted during explosive dacite events. Even during its ancestral period, Mount Pinatubo erupted andesite–dacite magmas (Newhall *et al.*, 1996). Although for the modern period it can be argued that the large silicic magma chamber has intercepted any ascending mafic batches, preventing them from reaching the surface, this argument does not hold for the ancestral and less mature period of the volcano, during which there were lower amounts of silicic derivatives and thus the probability of trapping mafic injections at depth was lower. It could be argued that basaltic lavas erupted at early stages have been eroded away, but given the size and longevity of the volcanic edifice, this appears highly unlikely. Density filtering or viscosity increase as a result of decompression-driven crystallization at mid- to upper-crustal levels may be other reasons for basalt stagnation at depth; however, we note that silicic arc magmas, for which the mafic–acid parental relationships have been convincingly shown, preserve abundant evidence for the physical mechanism of andesite–dacite production (e.g. Iztaccihuatl, Nixon, 1988; Mt Pelée, Pichavant *et al.*, 2002a).

Altogether, the geological record and experimental– geochemical constraints do not favour a low-pressure basalt fractionation model for the Pinatubo dacite. Contrary to many other calc-alkaline volcanoes (e.g. Nixon, 1988; Feeley & Hacker, 1996; Clynne, 1999; Pichavant *et al.*, 2002a), there is no widespread textural or chemical evidence at Pinatubo for a significant fraction of 1991 dacite phenocrysts being either derived from previous magma mixing events between magmas with contrasted compositions or inherited from a deeper stage of magma evolution. Any mafic magma injections must have thus consisted mainly of small magma batches that with time were mixed with the chamber magma and disaggregated into single isolated minerals (e.g. Clynne, 1999), having little impact on the geochemical evolution of the dacite pluton. Apart from the occasional presence of olivine and bronzite xenocrysts (Pallister *et al.*, 1996), the sole, albeit important, exceptions are provided by the occurrence of high-Al hornblende and rare calcic plagioclase, which together represent <1% of the volume of phenocrysts, and whose origin and implications are discussed in this paper.

# EXPERIMENTAL PROCEDURE

## Starting materials and charges

Experiments were of two types: dacite crystallization at 400 and 960 MPa, and dacite–peridotite interaction at 920 MPa. For the crystallization experiments, the strategy followed was similar to that of previous phase equilibrium studies of felsic magmas (e.g. Green, 1972; Pichavant, 1987; Conrad *et al.*, 1988; Holtz *et al.*, 1992; Scaillet *et al.*, 1995; Scaillet & Evans, 1999) in which dry glasses are used as starting material. This dry glass was obtained by fusing the dacite rock powder (Table 1) in a Pt crucible for about 4 h at 1400°C in air. Melting was done twice with grinding in between and the resulting glass was analysed by electron microprobe, showing no significant differences from the whole-rock wet chemical analysis (see Prouteau *et al.*, 1999; Scaillet & Evans, 1999). In particular, iron and sodium contents were similar to the bulk rock, showing that neither iron loss to the Pt crucible nor sodium volatilization occurred during melting. All experiments used Au capsules (inner diameter 2 mm; length 15 mm).

For dacite crystallization experiments, both water-saturated and water-undersaturated experiments were carried out. At 960 MPa, capsules were loaded with the silicate powder (glass or glass + crystals) plus distilled and deionized water in various proportions. At 400 MPa silver oxalate was used in addition to water to generate an H<sub>2</sub>O–CO<sub>2</sub>–fluid, with a fluid/glass weight ratio of 15/85.

For the dacite–peridotite interaction experiments, the charges consisted of the dacite glass powder mixed with mantle olivine, orthopyroxene and clinopyroxene. The mantle minerals were separated from a sample of San Carlos peridotite and then crushed to a 60–80 µm mesh size. We tested the effects of adding olivine only, olivine + orthopyroxene, and olivine + orthopyroxene + clinopyroxene, to the dacite end-member, to assess the effects of changing mantle lithology (residual or fertile). Glass powder and mantle minerals, with a weight ratio of ~60/40, were carefully mixed and loaded in the capsules together with ~7 wt % distilled and deionized water.

All capsules were arc-welded and checked for leaks by immersion in an oil bath at 120°C. Runs were performed with up to seven capsules (charges with different H<sub>2</sub>O contents at 960 MPa or different H<sub>2</sub>O/CO<sub>2</sub> ratios at 400 MPa) kept together under the same  $P$ – $T$ – $f_{H_2}$  conditions and same durations.

## Equipment and run procedures

Experiments were carried out in internally heated pressure vessels (IHPV) with either Ar–H<sub>2</sub> mixtures (400 MPa) or Ar (830–980 MPa) as a pressure medium. For the latter, excluding the 830 MPa run, average pressures for the crystallization and interaction experiments are 960 MPa (crystallization) and 920 MPa (interaction), respectively. Because the 830 MPa run results are in good agreement in terms of phase assemblage and phase composition with experiments performed in the pressure range 920–980 MPa, they have been also used for establishing the phase relations and compositional trends. Thermal gradients across the charges were mostly <2°C. Temperature and pressure are accurate to within ±5°C and 20 bar, respectively. The experiments at 400 MPa were ended with a drop-quench technique (Roux & Lefèvre, 1992), with a temperature drop of ~100°C/s; those at 960 MPa by switching off the power supply, inducing temperature drops of ~100°C/min. Experimental durations varied between 50 and 309 h, decreasing with rising temperature. After the experiment, capsules

were weighed to check for leaks and opened. For each charge, a fragment of the run product was embedded in epoxy resin and polished.

### **Control of $f_{O_2}$**

The oxygen fugacity [reported in Table 2 in log values relative to the NNO buffer and calculated at the pressure of interest using the calibration of Pownceby & O'Neill (1994)] was controlled using Ni–Pd–NiO and Co–Pd–CoO solid-state sensors (Taylor *et al.*, 1992; Pownceby & O'Neill, 1994), the preparation of which has been detailed by **Scaillet & Evans** (1999). Sensor compositions were found to be homogeneous within analytical uncertainties, except for the experiments performed at 960 MPa and 890°C, for which the results have been found to be unreliable (i.e. the Ni concentration as determined by electron microprobe varied erratically across the charge, preventing any meaningful average to be calculated); the  $f_{O_2}$  of these experiments has been interpolated using the results obtained at 840°C and 950°C, 960 MPa. For water-undersaturated charges, the water dissociation reaction was used to compute  $f_{O_2}$  from the experimental  $f_{H_2}$  and calculated  $f_{H_2O}$  (**Scaillet et al.**, 1995). The water fugacity of the charges has been calculated using the model of Silver *et al.* (1990), which allows calculation of the  $f_{H_2O}$  knowing the melt H<sub>2</sub>O concentration.

### **Analytical methods**

Run products were characterized by electron microprobe (EMP) and scanning electron microscopy (SEM). The major elements were analysed with a Cameca SX 50 (Services Communs BRGM–CNRS, Orléans), at an acceleration voltage of 15 kV, a counting time of 10 s and a sample current of 6 nA. Beam sizes of 1–2 µm were employed for mineral phases and a defocused beam of 5 or 10 µm for glasses. The measured alkali concentrations of the glasses were corrected by using secondary standards of dacitic and rhyolitic compositions with known alkali and water contents (**Scaillet et al.**, 1995). The water contents of the experimental glasses were determined by using the summation deficit to 100% of the EMP analyses method (Devine *et al.*, 1995), using eight dacitic to rhyolitic standard glasses containing up to 9.1 wt % H<sub>2</sub>O as determined by Karl Fisher titration or ion-microprobe analysis (**Scaillet et al.**, 1995; Martel *et al.*, 1998). No effort was made to determine the CO<sub>2</sub> content of quenched glasses at 400 MPa. However, the established low solubility of CO<sub>2</sub> in silicic melts at mid- to lower-crustal pressures (e.g. Fogel & Rutherford, 1990) suggests that the CO<sub>2</sub> content in these charges is unlikely to exceed 1000 ppm, and consequently that the CO<sub>2</sub> effect on phase relations occurs merely through a decrease of H<sub>2</sub>O activity in the coexisting fluid phase.

## **EXPERIMENTAL RESULTS**

### **Run products and phase proportions**

#### *Crystallization experiments*

Experimental conditions and run products are given in Table 2. Run products consisted of glass and mineral phases including amphibole, clino- and orthopyroxene, plagioclase, quartz and Fe–Ti oxides. No textural evidence of quench crystallization was found, except in the case of the H<sub>2</sub>O-saturated run at 960 MPa (PIN110, Table 2) in which minute crystals of quench hornblende were present. Phase proportions calculated by mass balance yield low residuals (Table 2), showing that glasses were correctly analysed and that no major phase was missing.

Plagioclase is the most abundant mineral phase for the lower melt water contents and temperature (Table 2). It has a thin tabular shape and its grain size increases with H<sub>2</sub>O<sub>melt</sub> and rise in temperature between 5 and 30 µm. At fixed pressure both a rise in temperature and

increase in melt water content lead to a decrease of plagioclase abundance. For example, at 960 MPa, there is ~5 wt % plagioclase at 945°C and ~7 wt % H<sub>2</sub>O in melt (H<sub>2</sub>O<sub>melt</sub>), and 42 wt % plagioclase at 840°C, for the same melt water content. Amphibole has a euhedral shape with a grain size varying between 10 and 50 µm; it is free of inclusions. In contrast to plagioclase, the proportion of amphibole is roughly constant at 8–12 wt % over most its stability field, only decreasing to ~5 wt % close to the liquidus, in concert with a complementary increase in clinopyroxene (960 MPa) or clinopyroxene ± orthopyroxene (400 MPa). Magnetite is constant at 3–4 wt % over the *P–T–H<sub>2</sub>O<sub>melt</sub>* interval studied and only traces of ilmenite were detected. At fixed *P*, the amount of glass decreases monotonously with decreasing H<sub>2</sub>O<sub>melt</sub> and temperature. For example, at 960 MPa and 890°C, the glass proportion decreases from ~88 wt % at H<sub>2</sub>O-saturation to ~58 wt % for H<sub>2</sub>O<sub>melt</sub> ~6 wt %; and at 960 MPa and H<sub>2</sub>O<sub>melt</sub> ~7 wt % from 83 wt % at 940°C to ~31 wt % at 840°C (Table 2).

### *Interaction experiments*

Experimental conditions and run products are given in Table 3. In addition to glass, run products contain the mantle mineral phases initially loaded (i.e. olivine ± orthopyroxene ± clinopyroxene) plus new orthopyroxene (labelled Opx2 in Table 3), amphibole and, in one charge, phlogopite (Table 3), all phases that grew during interaction at *P* and *T*. No olivine nucleated during the experiments, and olivine seeds contained abundant minute oxide inclusions, perhaps owing to the high prevailing oxygen fugacity that produced oxide exsolution during the experiments. The amphibole and phlogopite sizes range between 15 and 80 µm with an average at 30 µm. In all runs, the most abundant new phase is orthopyroxene, which occurs commonly as overgrowths on original orthopyroxene and as reaction coronas around olivine crystals.

### **Phase relations of the Pinatubo dacite**

The phase relations at 400 MPa are shown in Fig. 1a. At H<sub>2</sub>O<sub>melt</sub> >7 wt %, amphibole is the liquidus silicate phase. At lower melt H<sub>2</sub>O contents, it is replaced by clinopyroxene and then orthopyroxene. Although amphibole and pyroxenes coexist in some runs, their relationship is that of a peritectic reaction. The amphibole-out curve shows a thermal maximum (~950°C) for H<sub>2</sub>O<sub>melt</sub> of 6–7 wt % and thus its maximum thermal stability is not at H<sub>2</sub>O-saturation, in agreement with theoretical analyses (Eggler, 1972; Holloway, 1973; Ghiorso, 1999). Plagioclase is the first tectosilicate to crystallize, with a liquidus temperature around 900°C for water-saturated conditions. At H<sub>2</sub>O-saturation, quartz crystallizes around 750°C and its saturation curve is roughly parallel to that of plagioclase. Magnetite is present throughout the entire studied crystallization interval: its upper stability has not been determined and the position of the magnetite-out curve is only approximate. Ilmenite crystallizes at around 800°C at H<sub>2</sub>O-saturation (Scaillet & Evans, 1999). Because it occurs sporadically in the experimental run products above 800°C, the saturation curve for ilmenite is also approximate and shown dashed.

The phase relations at 960 MPa are shown in Fig. 1b, displaying a similar topology to those at 400 MPa. Magnetite is the liquidus phase, followed by clinopyroxene, except in the most water-rich experiments, where amphibole replaces clinopyroxene. Amphibole is stable up to 970°C for H<sub>2</sub>O<sub>melt</sub> >7 wt % and its thermal stability decreases at lower H<sub>2</sub>O<sub>melt</sub>. No clinopyroxene was observed in runs performed at 840°C and 750°C, suggesting that the stability domain of clinopyroxene below 900°C, if any, is restricted to very dry conditions. Accordingly, we suggest that clinopyroxene displays a peritectic relationship with amphibole in the water-rich part, as observed at 400 MPa. Such a relationship between amphibole and pyroxenes has also been found in granitic systems (e.g. Naney, 1983; Dall'Agnol *et al.*, 1999).

It suggests that in hydrous silicic to dacitic magmas cooling at pressures higher than 150 MPa, pyroxenes react out to amphibole before solidus conditions are attained.

The comparison between the 400 and 960 MPa isobaric sections shows that the relative order of crystallization remains unchanged in this pressure range. The liquidus temperatures of the tectosilicates fall by  $\sim 25^{\circ}$ – $75^{\circ}$ C as pressure increases from 400 to 960 MPa. Altogether, the main effect of increasing pressure is to destabilize orthopyroxene, which is not stable in dacite at 960 MPa under high  $f_{O_2}$ . Orthopyroxene is the dominant pyroxene at 220 MPa (Scaillet & Evans, 1999) and it coexists with clinopyroxene in approximately equal relative proportions at 400 MPa.

## Phase compositions

### *Plagioclase*

The compositions given in Table 4 are average analyses, selected on the basis of a total close to 100% and on the correctness of the structural formula. A number of analyses contain appreciable Fe (up to 2 wt % as  $FeO_{tot}$ ), partly because of the presence of minute oxide inclusions, as observed in other crystallization experiments (e.g. Dall'Agnol *et al.*, 1999) but also because of the substitution of  $Al^{3+}$  by  $Fe^{3+}$  owing to the high  $f_{O_2}$  of the experiments. The plagioclase composition shows systematic variations with the experimental parameters. At fixed  $P$ , the anorthite component of plagioclase increases systematically with rise in temperature and decreases with falling  $H_2O_{melt}$  (Table 4 and Fig. 2). The effect of  $H_2O_{melt}$  on the anorthite content is greater at high temperatures (Fig. 2). At constant temperature and bulk  $H_2O$  content, the plagioclase becomes more sodic with increasing pressure (Fig. 2). The most calcic plagioclase observed in this study is  $An_{62}$  (Table 4).

The molar ratio  $(Ca/Na)_{plag}/(Ca/Na)_{liq}$  ( $K^{Ca/Na}$ ) varies between 2.7 and 3.2 at 400 MPa and between 1.2 and 3.2 at 960 MPa (Table 4), well below the  $K^{Ca/Na}$  for  $H_2O$ -saturated basaltic to dacitic liquids at 200 MPa ( $\sim 5.5$ , Sisson & Grove, 1993). At 960 MPa,  $K^{Ca/Na}$  increases with rise in temperature (Table 4), but there is apparently no correlation between  $K^{Ca/Na}$  and  $H_2O_{melt}$ , as found in other experimental studies at lower pressures (e.g. Sisson & Grove, 1993).

### *Amphibole*

Amphibole compositions are listed in Table 5. Structural formulae are calculated for 23 oxygens. Calculations using the  $Si + Al + Fe + Mg + Mn + Ti = 13$  constraint [the sum of cations other than Ca, Na and K is taken to be equal to 13; see Leake *et al.*, (1997)] suggest that  $Fe^{3+}$  proportion varies between 30 and 80% of total iron.

### *Crystallization experiments*

The amphibole composition appears to be homogeneous on the basis of several grains in each charge and an average amphibole composition is reported in Table 5. It is a calcic and aluminous amphibole, classified as magnesio-hornblende or tschermakitic hornblende (Leake *et al.*, 1997) but for simplicity the name hornblende is used. The composition of hornblende is sensitive to all experimental variables. The total Al shows a broad positive correlation with pressure. At fixed  $P$  and  $H_2O_{melt}$ , a rise in  $T$  produces a small but significant increase in Ca and a decrease in Si (Table 5), as well as an increase in Na + K (Fig. 3b). The Mg number range is between 0.78 and 0.83 at 400 MPa, 0.70 and 0.84 at 960 MPa (except for PIN102, Mg number = 0.60) (Table 5). The Ti content varies from 0.10 to 0.16 p.f.u. at 400 MPa, and from 0.08 to 0.12 p.f.u. at 960 MPa. Both the Mg number and Ti contents are insensitive to either temperature or  $H_2O_{melt}$ , in the range of  $f_{O_2}$  investigated (Fig. 3c and d). The lack of

temperature dependence may be due to the high proportions of Fe–Ti oxides (see Helz, 1982). As found in earlier studies (Helz, 1982), the Mg number, and to a lesser extent the Ti content, are sensitive to the  $f_{O_2}$ . The high Mg number and low Ti contents of hornblendes at 400 and 960 MPa are the consequence of the high  $f_{O_2}$  of the experiments. The higher Mg number of the hornblende produced at 750°C and 960 MPa reflects the higher  $f_{O_2}$  of this experiment relative to others at the same pressure (Fig. 3c). Also plotted in Fig. 3 are hornblendes from the experiments of Conrad *et al.* (1988) performed on the Taupo dacite (Table 1) at 1000 MPa but at a lower  $f_{O_2}$ , close to that defined by the fayalite–magnetite–quartz solid buffer (FMQ). As expected, low- $f_{O_2}$  hornblendes have significantly lower Mg number and higher Ti contents than those synthesized at high  $f_{O_2}$  (Fig. 3c and d). Finally, increasing pressure results in an increase in total Al content (Fig. 3a), as found in other studies (e.g. Hollister *et al.*, 1987; Johnson & Rutherford, 1989; Schmidt, 1992).

#### *Interaction experiments*

Amphibole displays significant compositional variations in individual charges and therefore analyses have not been averaged (Table 5). Most amphiboles are magnesio-hornblende or magnesio-hastingsitic hornblende, after Leake *et al.* (1997), with Mg number between 0.79 and 0.93 (Table 5). A rise in temperature decreases Si and increases Ca contents (Table 5). At a fixed temperature, the composition of amphibole does not vary with the modal composition of the ultramafic assemblage (Fig. 3), except when only olivine is involved, in which case a more alkali-rich amphibole is produced (As10 and As26, Fig. 3); at 950°C, this amphibole is associated with phlogopite. Relative to the amphibole produced in the 960 MPa Pinatubo dacite crystallization experiments, the amphibole in the interaction experiments has a lower Al content (Fig. 3a) and significantly higher alkali contents (Fig. 3b). Ti contents and Mg number display almost the same range of variation in the two types of experiments (Fig. 3c and d).

#### *Phlogopite*

Phlogopite is present in only one interaction run (As10: 920 MPa, 950°C). Individual analyses are listed in Table 6. Phlogopite is characterized by high  $Al_2O_3$  (14.5–16.8 wt %) and  $Na_2O$  (1.3–1.9 wt %) contents. Its Mg number ranges from 0.88 to 0.90 (Table 6).

#### *Clinopyroxene*

The compositions of the experimental clinopyroxenes are listed in Table 7 and shown in Fig. 4. The Ca-rich clinopyroxene synthesized at 400 and 960 MPa is an augite or a salite with a composition in the range  $En_{36-44}Wo_{42-50}Fs_{10-17}$ . It has an  $Na_2O$  content of 0.88–1.21 wt %,  $Al_2O_3$  5.03–7.65 wt % and  $TiO_2$  0.31–0.91 wt %. It has high Mg number, between 0.71 and 0.81. At fixed  $P$  and  $T$ , an increase of  $H_2O_{melt}$  produces an increase in Ca and, to a lesser extent, in the Na content of the clinopyroxene (Fig. 4). At fixed  $H_2O_{melt}$ , rising temperature increases slightly the Ca content of the clinopyroxene. Again, as expected, clinopyroxene produced at 1000 MPa in the more reduced experiments of Conrad *et al.* (1988) has a lower Mg number (mostly ranging from 0.55 to 0.62) than that synthesized in our oxidizing 960 MPa experiments (0.71–0.81, Table 7). It is also less calcic and sodic than the clinopyroxene synthesized at high  $f_{O_2}$ , all other parameters being similar (Fig. 4a and b).

### *Orthopyroxene*

Compositions of orthopyroxene produced in the interaction experiments are listed in Table 8. As for amphibole, orthopyroxene displays significant compositional variations within a single charge and analyses have not been averaged. It is an enstatite or a bronzite with composition in the range  $\text{En}_{82-95}\text{Wo}_{1-3}\text{Fs}_{5-16}$ . The compositions show no systematic variation with varying temperature or peridotite composition. Both Fe and Mg enrichment ( $\text{En}_{82-95}$ ) relative to the starting orthopyroxene ( $\text{En}_{88}$ ) is observed in a single charge. Overgrowths on original orthopyroxene display frequently complex zonation, with an inner zone enriched in Fe and an outer zone enriched in Mg, compared with the original orthopyroxene. Orthopyroxene overgrowths and newly nucleated orthopyroxene display the same compositional variation range (Table 8).

### *Fe–Ti oxides*

Compositions of 400 and 960 MPa Fe–Ti oxides are reported in Table 9. Magnetites are titanomagnetites with  $\text{TiO}_2$  up to 10.3 wt %. They contain significant  $\text{Al}_2\text{O}_3$  (1.0–3.0 wt %) and MgO (1.2–3.2 wt %). The proportion of ulvöspinel, calculated after Stormer (1983), increases with decreasing  $\text{H}_2\text{O}_{\text{melt}}$  and fall in temperature (Table 9). Ilmenites analysed in charges PIN100 and PIN104 are hemoilmenite with  $\sim 33.5$  wt %  $\text{TiO}_2$ .

### *Glasses*

#### *Crystallization experiments*

The compositions of glasses are listed in Table 10. In all analysed charges, the glass is homogeneous within analytical uncertainty. It has a composition ranging from rhyodacitic to rhyolitic, depending on experimental conditions. The melt water content at  $\text{H}_2\text{O}$ -saturation is estimated to be close to 9 wt % at 400 MPa (at 900°C), increasing to  $\sim 13$  wt % at 960 MPa (at 900°C). Glasses show systematic compositional variations with progressive crystallization: at fixed  $P$ , falling temperature or decreasing melt water content produce an increase in  $\text{SiO}_2$  and  $\text{K}_2\text{O}$  and a decrease in  $\text{Al}_2\text{O}_3$ , CaO and, to a lesser extent, MgO and FeO contents (Fig. 5). On average, the melts produced at 960 MPa are less silica-rich than those produced at 400 MPa (Fig. 5), owing to the increasing water solubility with pressure and lower crystallinity of the run products.

The CIPW (wt %) normative components of the glasses have been projected into Ab–An–Or and Ab–Qz–Or diagrams (Figs 6 and 7). The compositions of glasses produced at 220 MPa (Scaillet & Evans, 1999) and those of Conrad *et al.* (1988) are also shown. On the Ab–An–Or projection, an isothermal increase in  $\text{H}_2\text{O}_{\text{melt}}$  at 220 and 400 MPa drives the residual liquid away from the Or apex toward higher anorthite contents. At 400 MPa, above the saturation curve of plagioclase, the glasses evolve with a nearly constant Ab/Or ratio (Fig. 6b). The melt evolution is controlled either by amphibole breakdown (900°C) or by amphibole and clinopyroxene breakdown (950°C). In the temperature range 780–950°C, the 220 or 400 MPa liquid lines of descent define a single trend, which shows that, in terms of normative salic components, pressure with variations in this range has little effect on the compositional evolution of magmas with dacitic bulk compositions.

At 960 MPa, an increase in  $H_2O_{\text{melt}}$  increases the normative An content and decreases the Or content (Fig. 6c), as observed at lower pressures. However, in contrast to the coherent melt compositions observed at 220 and 400 MPa, it is not possible to define a single liquid line of descent (LLD), glass compositions spreading sub-parallel to the Ab–Or join, with low-temperature glasses lying on the Or-rich side. This observation, also apparent in the experiments of Conrad *et al.* (1988) (Fig. 6d), is the consequence of the higher stability of ferromagnesian phases (amphibole, clinopyroxene) relative to tectosilicates at high water pressures and  $f_{O_2}$ . For temperatures below 900°C and  $H_2O$ -rich conditions, plagioclase is absent or present in very low proportions, explaining the more An-rich character of the residual melts at 960 MPa, relative to those obtained at similar temperatures but lower pressures. At higher temperatures (>900°C), this effect is compensated by extensive clinopyroxene crystallization for low  $H_2O_{\text{melt}}$ . Thus, at pressures higher than 400 MPa, the liquid line of descent of dacite magmas is controlled by the relative proportions of plagioclase and ferromagnesian phases crystallizing, whereas below 400 MPa plagioclase appears to be the dominant phase controlling the residual melt composition.

The Ab–Qz–Or projection (Fig. 7) shows an increase in Qz component as temperature falls or  $H_2O_{\text{melt}}$  decreases at all pressures (Fig. 7). In the pressure range 220–400 MPa, the liquid lines of descent are again nearly superimposed on each other, defining a single array that trends away from the Ab apex at nearly constant Or/Qz normative ratios with falling temperature (Fig. 7a and b). At 960 MPa, however, the crystallization of quartz stops this increase, glasses trending either parallel to the Ab–Or join or toward the Or apex (Fig. 7c). The glasses of Conrad *et al.* (1988) show the same disposition (Fig. 7d).

The  $FeO^*/MgO$  ratios (where  $FeO^*$  is total Fe as FeO) of the experimental liquids vary from 0.9 to 3.9 at 400 MPa and from 1.1 to 2.6 at 960 MPa (Table 9), and increase with the  $SiO_2$  content of the glass (Fig. 8). The compositions plot in the calc-alkaline field and follow the trend defined by typical calc-alkaline rock suites (Fig. 8). Amphibole and clinopyroxene display significantly higher Mg number than the coexisting rhyodacitic melts (0.69–0.84 and 0.71–0.81 in amphibole and clinopyroxene, respectively, vs 0.26–0.53 in quenched melts; Tables 4–7), a result of high- $f_{O_2}$  conditions that, by promoting massive crystallization of Fe–Ti oxides, prevent iron enrichment and buffer the  $FeO^*/MgO$  of residual melts to low values (e.g. Sisson & Grove, 1993; Pichavant *et al.*, 2002a). The reduced experiments of Conrad *et al.* (1988) show a much stronger increase in  $FeO^*/MgO$  during crystallization (Fig. 8).

#### *Interaction experiments*

The average compositions of glasses are listed in Table 10. In all charges, the glass is homogeneous within analytical uncertainty. It has a rhyolitic composition and is peraluminous. Melt water contents are in the range 11.5–13.5 wt %. Falling temperature produces a slight decrease in  $Al_2O_3$  and, to a lesser extent,  $SiO_2$  and  $K_2O$  contents (Fig. 5). At a fixed temperature, the peridotite modal composition has little effect on the glass compositions, which are very similar within analytical uncertainty (Fig. 5). The comparison with the 960 MPa Pinatubo dacite melts shows that peridotite assimilation increases  $SiO_2$  and  $Al_2O_3$ , and decreases CaO,  $Na_2O$  and MgO, whereas  $K_2O$ , FeO and  $TiO_2$  remain unchanged (Fig. 5, Table 10).

# DISCUSSION

## General

For the crystallization experiments, the experimental procedure adopted in this study is identical to that of previous experimental work on silicic to intermediate magmas (e.g. Green, 1972; Pichavant, 1987; Conrad *et al.*, 1988; Martel *et al.*, 1998; Pichavant *et al.*, 2002a) and is known to favour attainment of equilibrium. The systematic geochemical trends displayed by both glass and minerals and their coherent variations with experimental variables also argue that conditions close to equilibrium were attained. In contrast, for the interaction experiments, the homogeneity of glass composition and heterogeneity of crystal chemistries and textures suggest that only local equilibrium conditions were reached.

The comparison with the phase diagram of Conrad *et al.* (1988) shows overall good agreement in terms of crystallization temperatures and phase topology in the dacite–H<sub>2</sub>O system. The main difference concerns the orthopyroxene. Whereas orthopyroxene is stable at low  $f_{O_2}$ , it was not detected in any of our 960 MPa experiments. This suggests that, at high pressure, orthopyroxene occurrence in dacite magma is critically dependent on oxygen fugacity (see Green, 1992), its stability being enhanced at low  $f_{O_2}$  (see also Dall'Agnol *et al.*, 1999).

Garnet was not produced in either our 960 MPa experiments or in those of Conrad *et al.* (1988) on the Taupo dacite; yet in the same study Conrad *et al.* (1988) crystallized garnet in a more peraluminous, but still dacitic (termed greywacke in Table 1) composition, which suggests that garnet absence in our experiments is not linked to high  $f_{O_2}$ . Green (1982, 1992) noted that melts with low normative diopside crystallize near-liquidus garnet at lower pressures than those that are diopside-rich. In the experiments of Green (1992) on the Taipa garnet-bearing dacite (Table 1), which has low normative diopside (0.7%), garnet is stable at 8 kbar, 850°C, 3 wt % H<sub>2</sub>O. We therefore conclude that garnet absence in both Pinatubo (3.3% normative diopside) and Taupo dacites reflects its intrinsic instability in these compositions, as a result of their high normative diopside content (Green, 1992). Pressures higher than 1000 MPa are probably needed to crystallize garnet in Pinatubo-like dacite compositions.

## Origin of calcic plagioclase and high-Al<sub>2</sub>O<sub>3</sub> hornblende

At no pressure does plagioclase as calcic as An<sub>80</sub> crystallize directly from the dacite. This implies that those rare An<sub>80</sub> plagioclases found in the dacite (Hattori & Sato, 1996) must be xenocrysts: they are probably inherited from previous basalt–dacite mixing events.

Various hypotheses can be proposed for the high-Al<sub>2</sub>O<sub>3</sub> hornblende. However, as oxygen isotope data preclude a significant contamination of dacitic magma by the Zambales complex (Fournelle *et al.*, 1996), only two possibilities are left to explain the high-Al<sub>2</sub>O<sub>3</sub> hornblende cores: they represent either remnants of dacite–basalt interaction events (e.g. Fournelle *et al.*, 1996) or a high-pressure crystallization stage. The use of Al vs Na + K and Al vs Mg number diagrams (Fig. 9) leads us to favour the second possibility. As stated above, the hornblende in the dacite falls into two groups: a low-Al and a high-Al group (Table 11). The hornblende in the andesite resembles either the low-Al<sub>2</sub>O<sub>3</sub> hornblende in the dacite or the hornblende in the basalt (Fig. 9), in agreement with the mingled status of the andesite magma (Pallister *et al.*, 1996). The hornblende in the basalt plots largely outside the field defined by the high-Al<sub>2</sub>O<sub>3</sub> hornblende in dacite, being Ca-, Al-, Na- and K-rich (Fig. 9), as well as distinctly Si-poor (Si ~6 p.f.u.). The fact that the fields defined by the hornblende in basalt and dacite do not overlap makes it difficult to propose basalt as the ultimate source of the high-Al<sub>2</sub>O<sub>3</sub> hornblende in

dacite. In contrast, the high- $\text{Al}_2\text{O}_3$  hornblende in the dacite is either partially or fully reproduced by the dacite crystallization experiments at 400 and 960 MPa (Fig. 9), therefore supporting a high-pressure origin for these hornblendes. The high Mg number of the high- $\text{Al}_2\text{O}_3$  hornblende points to oxidizing conditions during crystallization, as it is reproduced under high  $f_{\text{O}_2}$  whereas the hornblende produced in the reduced experiments of Conrad *et al.* (1988) has lower Mg number, from 0.42 to 0.63 (Fig. 9). This shows that the oxidized character of the dacite was acquired very early in the magmatic history (see Scaillet & Evans, 1999).

The above observations suggest that the dacite magma may have experienced crystallization in the range 400–960 MPa, before final emplacement in the upper reservoir at 200 MPa where most of the crystallization occurred. By implication, the fact that the magma was within the  $P$ – $T$  stability field of hornblende indicates that temperature during this high-pressure event was not higher than 900–950°C (Fig. 1). This implies also that  $\text{H}_2\text{O}_{\text{melt}}$  was already high during this early stage, with a minimum of 5–6 wt %  $\text{H}_2\text{O}_{\text{melt}}$  for hornblende to crystallize and possibly  $\text{H}_2\text{O}_{\text{melt}}$  higher than 10 wt % to be outside the clinopyroxene stability field at 960 MPa (Fig. 1), as clinopyroxene is absent even in the core of amphibole phenocrysts.

#### **Additional constraints on dacite $P$ – $T$ – $\text{H}_2\text{O}$ conditions during ascent**

The plagioclase crystallized at 400 and 960 MPa displays trends that are displaced toward higher Or contents than the natural one, especially at An >40 mol % (Fig. 10). At 400 MPa and moderate temperatures (785–900°C), plagioclase has a higher Or content (up to 4.6 mol %), even at high  $\text{H}_2\text{O}_{\text{melt}}$ , than the natural dacite plagioclase. The same is true at 960 MPa: plagioclase synthesized at low temperatures and low  $\text{H}_2\text{O}_{\text{melt}}$  is Or-rich (up to 4.8 mol % at 840°C). High  $\text{H}_2\text{O}_{\text{melt}}$  (e.g. 10.5 wt % at 840°C) and/or high temperature are necessary to match the natural trend (Fig. 10). However, temperatures significantly higher than 950°C are unlikely, as amphibole would be unstable under these conditions (see above). Had the Pinatubo dacite crystallized Or-rich plagioclase, then we would expect to find some Or-rich cores, unless diffusive re-equilibration erased them. These observations do not exclude the possibility of high-pressure plagioclase crystallization, but constrain this crystallization stage to have occurred at high  $\text{H}_2\text{O}_{\text{melt}}$ .

Figure 11 illustrates the evolution of  $\text{Al}_2\text{O}_3$  vs  $\text{SiO}_2$  contents of the Pinatubo glass inclusions, mostly found in plagioclase, and of experimental glasses produced at 960, 400 and 220 MPa. The 960 MPa experimental glasses are less evolved than the plagioclase glass inclusions. At 400 MPa, 900 and 950°C, the experimental melts similar to natural glass inclusions have  $\text{H}_2\text{O}$  concentrations (~4.3 wt %, Table 8) lower than those preserved in the natural melt inclusions (6–7 wt %, Gerlach *et al.*, 1996; Rutherford & Devine, 1996). The overlap between the 220 MPa experimental glasses and the glass inclusions suggests that the latter were mainly trapped at low pressures, indicating in turn that the Pinatubo dacite plagioclase crystallized predominantly in the shallow-level reservoir, as its composition suggests.

Figure 12 shows the amphibole and plagioclase saturation curves in a pressure–temperature diagram for various bulk  $\text{H}_2\text{O}$  contents using the 400 and 960 MPa experimental constraints of this study (Table 2) and the 220 MPa data of Scaillet & Evans (1999). Melting experiments performed on the Pinatubo dacite show that melting of amphibole takes a few days or even a few hours (Rutherford & Devine, 1996) when temperature exceeds 900°C. Therefore, the likelihood of preservation of high-pressure hornblende if the magma ascent trajectory intersects the hornblende saturation curve during ascent is very poor, given the cooling time interval of a magmatic body of such dimensions (>90 km<sup>3</sup>, Mori *et al.*, 1996). Figure 12

shows that magma temperatures of  $\sim 900^\circ\text{C}$  (path 1) during adiabatic ascent are needed to preserve high-pressure hornblende up to shallow levels. A  $900^\circ\text{C}$  magma lies continuously within the amphibole stability field during its ascent to the surface whatever the water content considered (Fig. 12). For  $\text{H}_2\text{O}$ -saturated conditions the magma lies outside the plagioclase stability field up to 380 MPa (Fig. 12a). If the magma contains  $\sim 10$  wt %  $\text{H}_2\text{O}$ , plagioclase appears at  $\sim 400$  MPa (Fig. 12b). For any  $\text{H}_2\text{O}$  content lower than this threshold, the dacite crystallizes plagioclase in addition to hornblende during its entire ascent (Fig. 12c), which is not supported by the petrological and phase chemistry evidence outlined above. The  $950^\circ\text{C}$  adiabat (path 2) continuously lies outside the hornblende stability field for water-saturated conditions (Fig. 12a) and recrosses the hornblende saturation curve for lower water contents (Fig. 12b and c).

Therefore, to preserve the evidence of high-pressure crystallization, a restricted set of  $T$ - $\text{H}_2\text{O}$  conditions is required. A magma rich in water at temperatures below  $900^\circ\text{C}$  will crystallize extensively to the extent that the crystal load may inhibit its ascent as a result of the increase in viscosity. A magma too hot upon emplacement ( $>900^\circ\text{C}$ ) will soon dissolve the high-pressure amphibole. We thus infer that the dacite magma was not much hotter than  $900^\circ\text{C}$  when injected in the upper reservoir and that its water content was possibly as high as 10 wt %. The fact that there is no amphibole with intermediate composition (Fig. 9) may be attributed to rapid ascent between stages 1 and 2. As a corollary it can be noted that, at 220 MPa, the magma was saturated in a fluid phase during the entire repose time before eruption.

### **Dacite origin**

Models for generating arc dacites include mixing between rhyolitic and more basic magmas, fractional crystallization of basaltic–andesitic magmas in the crust (Gill, 1981) or in the upper mantle (Green, 1992; Harangi *et al.*, 2001), melting of basaltic rocks either in the lower–upper crust (e.g. Smith & Leeman, 1987; Atherton & Petford, 1993; Costa & Singer, 2002) or within the subducted slab (e.g. Defant & Drummond, 1990; Drummond & Defant, 1990), contamination of mantle-derived magmas by a garnetiferous lower continental crust (Feeley & Hacker, 1996), and near-solidus melting of hydrous garnet or spinel lherzolite (Mysen & Boettcher, 1975). Mixing between basalt and rhyolite as a mechanism for producing the Pinatubo dacite is considered unlikely given that the mineralogical and petrological attributes preserved in the dacite are reproduced by the low-pressure phase equilibrium experiments (Scaillet & Evans, 1999). Because mixing is fundamentally a disequilibrium mechanism, we would expect to find widespread textural and mineralogical evidence of such a process had it played a major role in the petrogenesis of the dacite. Moreover, the felsic end-member has yet to be recognized (Bernard *et al.*, 1996). Likewise, extensive contamination of basalt by the continental crust seems to be precluded by the radiogenic isotope characteristics and low  $\text{K}_2\text{O}$  content of the dacite (Bernard *et al.*, 1996; Castillo & Punongbayan, 1996). The dacite shows significant fractionation between light REE (LREE) and heavy REE (HREE) abundances ( $\text{La}_\text{N}/\text{Yb}_\text{N} \sim 8$ , Bernard *et al.*, 1996) and HREE depletion relative to common intermediate arc rocks ( $\text{Yb}_\text{N} \sim 6$ , Bernard *et al.*, 1996). Garnet is so far the only petrologically significant mineral phase able to fractionate the LREE from the HREE. Phase-equilibrium studies of basaltic compositions have shown that garnet is not stable at pressures  $<1000$  MPa (e.g. Sisson & Grove, 1993; Pichavant *et al.*, 2002a), nor it is a liquidus phase in the dacite in the same pressure range [this study and Conrad *et al.* (1988)]. Thus, although mid-crustal fractionation of hydrous basalts may yield liquid derivatives similar to the composition of Pinatubo dacite (e.g. Pichavant *et al.*, 2002a), the necessity of garnet precipitation precludes a

low-pressure context for the generation of the Pinatubo magma, in agreement with the geological evidence summarized above. The remaining mechanisms at high pressure are considered below in greater detail, keeping in mind that the main target of any petrogenetic model seeking to explain the origin of Pinatubo dacite is the production of an oxidized water-rich dacite liquid at temperatures of 900–950°C.

#### *Partial melting of basalt lithologies*

Partial melting of amphibole-rich lower crust has been suggested for dacite genesis at Pinatubo (e.g. Bernard *et al.*, 1996) and Mount St. Helens (Smith & Leeman, 1987). However, the melt water contents of liquids produced by dehydration melting of amphibolites (e.g. Beard & Lofgren, 1991; Wolf & Wyllie, 1994; Rapp & Watson, 1995) barely exceed 5 wt %, except at very low melt fractions (<10 wt %), i.e. below 900°C (Fig. 13a and b), but then the produced melts are either too SiO<sub>2</sub>-rich (Fig. 13c) or Al<sub>2</sub>O<sub>3</sub>-rich (Fig. 13d), or too potassic.

Melting could affect the downgoing slab. Fluid-absent experiments on basalts at 2000–3000 MPa can yield dacitic liquids (e.g. Rapp *et al.*, 1991; Sen & Dunn, 1994a; Rapp & Watson, 1995), but at temperatures over 1000°C and, as at lower pressures, the H<sub>2</sub>O<sub>melt</sub> of such liquids is 5 wt % at best. The dehydration-melting liquids obtained at lower temperatures are rhyolitic in composition (e.g. composition SD-94 in Table 12). Because temperatures of ~1000°C or higher are highly unlikely to be reached in modern subduction zones (Peacock *et al.*, 1994), it is improbable that high-pressure dehydration melting of the downgoing oceanic plate can produce Pinatubo-like magmas. Melting of basalt under excess water conditions at 2000 MPa may yield dacitic melts but they are enriched in CaO (up to 7.5 wt %) and Al<sub>2</sub>O<sub>3</sub> (up to 20.9 wt %) relative to Pinatubo dacite (e.g. Prouteau *et al.*, 2001). Similarly, melts produced at 3000 MPa are trondhjemitic (Table 12) instead of dacitic.

Clearly then, melts so far produced by melting of basalts at 1000–3000 MPa under *T*–H<sub>2</sub>O conditions given by the petrological, chemical and phase equilibrium constraints detailed previously show severe major element differences from the Pinatubo dacite; this shows that such magmas are not direct melting products from amphibolite sources.

#### *The role of the mantle wedge*

Experimental studies have shown that the key features of silicic magmas contaminated by the peridotite at mantle pressures are an increase of their Mg number (Mg number 50–60) and a decrease of their SiO<sub>2</sub> content (e.g. Carroll & Wyllie, 1989; Rapp *et al.*, 1999; Prouteau *et al.*, 2001). Although both effects will partly bridge the gap between the Pinatubo dacite and experimental slab melts, all experimental hybridized melts do not reproduce Pinatubo dacite compositions if all elements are considered (Table 12). In addition, at upper-mantle pressures, the Pinatubo dacite is saturated in hornblende, magnetite and clinopyroxene, i.e. unlike the phase assemblage of metasomatized peridotites, lacking in particular orthopyroxene and olivine. The Pinatubo dacite shows no evidence of having equilibrated with the mantle wedge, a conclusion that is also demonstrated by the extensive changes observed in our interaction experiments, in which melt compositions not yet recognized at Pinatubo or elsewhere are produced.

Pinatubo dacite could be generated directly from hydrous melting of mantle peridotite (e.g. Mysen & Boettcher, 1975). However, as stressed above, the dacite phase equilibria at 960 MPa show that at upper-mantle pressures, such magmas are not in equilibrium with typical

mantle mineralogy. In addition, although higher relative to conventional arc dacites, the Ni and Cr contents of the Pinatubo dacite are too low to support a primary mantle origin, or would imply that the magmas underwent olivine fractionation to a significant extent, yet the dacite is not saturated in olivine at upper-mantle pressures. We conclude that direct mantle derivation is a model difficult to envision for the Pinatubo dacite.

#### *Dacite derivation from primitive basalt fractionation at upper-mantle pressures*

The dacite could have been produced by crystallization of a basaltic magma in the deep arc crust, which, at Luzon, is 30–35 km thick (Wu, 1979; Listanco *et al.*, 1997; Mooney *et al.*, 1998). The basalt co-erupted during the 1991 eruptions has higher trace element concentrations and a different isotopic composition than the dacite (Bernard *et al.*, 1996; Castillo & Punongbayan, 1996; Hattori & Sato, 1996; Pallister *et al.*, 1996), which exclude a cogenetic relationship. However, the dacite can be generated by fractionation of a non-erupted, but isotopically similar, mafic magma. Müentener *et al.* (2001) carried out crystallization experiments on primitive hydrous basalts and high-Mg number andesites at 1200 MPa in the temperature range 1030–1230°C. They obtained basaltic to andesitic liquids saturated with two pyroxenes ± spinel and, for the most crystallized charges of hydrous basalts, garnet and amphibole. Extrapolation of their experimental trend shows that dacite liquids would be produced in the range 900–950°C (Fig. 13), with water contents in excess of 10 wt %, coexisting with garnet and amphibole. The evolution of phase proportions with falling temperature shows that once amphibole and garnet appear, the amount of pyroxenes decreases, notably that of orthopyroxene, suggesting that garnet–amphibole might be in reaction relationship with pyroxenes upon cooling and increasing melt water content. Although the limited data available at high pressure preclude any conclusive statement, the experiments of Müentener *et al.* (2001) open the possibility that primitive arc basalts produce derivative dacitic liquids having a garnet imprint. Dacite generation at upper-mantle pressure from a garnet-bearing protolith has been also proposed by Green (1992) for the Taipa dacite in New Zealand [see also Harangi *et al.* (2001)]. As shown by the experiments of Müentener *et al.* (2001), to produce such dacite melts requires pressures of at least 1200 MPa, temperatures below 1000°C and water-rich conditions of the parent magma, of at least 3 wt %. In the Luzon arc, the source region of the dacite magma is therefore in the upper mantle.

We envision the following scenario for the genesis of the Pinatubo dacite. Partial melting occurs in the sub-arc mantle triggered by the input of either slab melt or hydrous fluids from the downgoing oceanic plate, with some sediment input, as required by Be isotope constraints (Bernard *et al.*, 1996). The hydrous basaltic melt migrates upward and ponds at lowermost-crust to upper-mantle conditions, where it crystallizes until garnet precipitates. The reason why the basalt melt ponds may be its H<sub>2</sub>O-rich character, which promotes extensive crystallization during decompression (e.g. Pichavant *et al.*, 2002b), or the fact that it intrudes the colder part of the mantle wedge, or both factors. Once dacite liquids are produced, they are extracted owing to their low density and viscosity as a result of their high H<sub>2</sub>O content, both factors contributing to efficient separation between parent and daughter magmas. It is proposed that dacite melts produced by crystal fractionation of primitive basalts retain high concentrations of compatible elements such as Ni and Cr, but also MgO, simply because of their direct derivation from a primitive basaltic parent, and also because profuse crystallization of both garnet and amphibole will dampen the role of other Ni- and Cr-consuming phases such as olivine, spinel or pyroxenes. In this respect, it has to be noted that high pressures are necessary not only for garnet crystallization but also to remove olivine from the liquidus. It is well established that decreasing pressure in H<sub>2</sub>O- and Mg-rich magma stabilizes olivine at the expense of pyroxenes on the liquidus (e.g. Kushiro, 1972; Nicholls &

Ringwood, 1973; Pichavant *et al.*, 2002b), which will not favour production of relatively Ni-, Cr- and Mg-rich silicic derivatives. Once extracted, the dacite liquid experiences a first limited arrest at  $\sim 1000$  MPa, i.e. close to the mantle–crust rheological boundary, where it crystallizes high-Al amphiboles. Then, because of its extreme buoyancy, it ascends to shallow levels and injects a reservoir that expands with time and erupts magmas with little geochemical diversity. The fact that the basaltic parent magmas remain at mantle or lower-crustal depths readily explains the scarcity of mafic compositions in the eruptive products of Mt Pinatubo. Mafic magmas reaching shallow levels, which intrude the dacite reservoir (Pallister *et al.*, 1996; Daag *et al.*, 1996), may represent less H<sub>2</sub>O-rich varieties that survive decompression and that were generated in the mantle wedge under different  $P$ – $T$ –H<sub>2</sub>O conditions (see Pichavant *et al.*, 2002b).

Although the above scenario can qualitatively account for both the major and trace element characteristics as well as the temperature and melt water content of the Pinatubo dacite, the lack of experiments below 1000°C in the basalt–H<sub>2</sub>O system studied by Müntener *et al.* (2001) prevents a rigorous quantitative evaluation of the behaviour of trace elements (REE, Ni, Cr, Sr). We therefore suggest that future experimental work focuses on the phase relationships of hydrous arc basalts above 1000 MPa, at low temperatures and under high  $f_{\text{O}_2}$ .

## CONCLUSIONS

Major element and phase petrology considerations allow us to rule out several scenarios for dacite generation at Mt Pinatubo. In particular, a pure slab melt origin can be discarded. Slab melting, although undoubtedly operative in some tectonic settings (e.g. Kepezhinskas *et al.*, 1995; Prouteau *et al.*, 2001), produces melt compositions far too different from Pinatubo-type dacites, and there appears to be no simple recognized way to bridge the marked compositional gap existing between these two magma types in convergent zone settings while keeping a dominant slab contribution. In the case of Pinatubo dacite, the slab input seems to be restricted to the fluid or melt that infiltrates the sub-arc mantle and triggers its melting, bringing the water necessary to produce H<sub>2</sub>O-rich mantle melts. In our model, the mass contribution of the oceanic slab to dacite petrogenesis is minor relative to that of the mantle wedge, of the order of 3–5 wt % if all the water has a slab origin. Thus, although the Pinatubo dacite resembles in almost all respects magmas postulated to have been dominantly produced via slab melting, its mode of production has more in common with conventional arc magma petrogenesis than with magmas proposed to originate by slab melting. The main difference relative to typical arc dacites appears to be the pressure of their source region. A similar model has been proposed for the petrogenesis of garnet-bearing dacites in New Zealand (Green, 1992) and in the Carpathian region (Harangi *et al.*, 2001), although in both cases crustal interaction is proposed as an additional factor. Magmas sharing the geochemical and petrological characteristics of the Pinatubo dacite possibly represent deep felsic derivatives of particularly water-rich mantle wedge basalts. Dacite occurrences having adakite-like characteristics may therefore be a superficial expression of H<sub>2</sub>O-rich conditions in the sub-arc mantle wedge (e.g. Green, 1992) rather than the direct evidence of convergent plate settings in which hot and young oceanic crust subducts and melts (Defant & Drummond, 1990).

## ACKNOWLEDGEMENTS

This study is part of the Ph.D. thesis of G.P. and has received financial support from the IT-CNRS programme. Continuous discussions with René Maury, Michel Pichavant and Fidel Costa about the origin and mechanisms of evolution of arc magmas were of great help in developing the model presented in this paper. The reviews of Othmar Müentener and Malcolm Rutherford, and the careful editorial handling of Marjorie Wilson and Alastair Lumdsen greatly helped in clarifying the manuscript and are gratefully acknowledged.

## REFERENCES

- Albarède, F. (1995). *Introduction to Geochemical Modeling*. Cambridge: Cambridge University Press, 543 pp.
- Arth, J. G., Barker, F., Peterman, Z. E. & Friedman, I. (1978). Geochemistry of the gabbro–diorite–tonalite–trondhjemite suite of southwest Finland and its implications for the origin of tonalitic and trondhjemitic magmas. *Journal of Petrology* **19**, 289–316.
- Atherton, M. P. & Petford, N. (1993). Generation of sodium-rich magmas from newly underplated basaltic crust. *Nature* **362**, 144–146.
- Barnes, C. G., Barnes, M. A. & Kistler, R. W. (1992). Petrology of the Caribou Mountain pluton, Klamath Mountains, California. *Journal of Petrology* **33**, 95–124.
- Beard, J. S. & Day, H. W. (1988). The Smartville intrusive complex, northern Sierra Nevada, California: the core of a rifted volcanic arc. *Geological Society of America Bulletin* **99**, 779–791.
- Beard, J. S. & Lofgren, G. E. (1991). Dehydration melting and water-saturated melting of basaltic and andesitic greenstones and amphibolites at 1, 3 and 6.9 kbar. *Journal of Petrology* **32**, 365–401.
- Bernard, A., Demaiffe, D., Mattielli, N. & Punongbayan, R. S. (1991). Anhydrite-bearing pumices from Mount Pinatubo: further evidence for the existence of sulfur-rich silicic magmas. *Nature* **354**, 139–140.
- Bernard, A., Knittel, U., Weber, B., Weis, D., Albrecht, A., Hattori, K., Klein, J. & Oles, D. (1996). Petrology and geochemistry of the 1991 eruption products of Mount Pinatubo (Luzon, Philippines). In: Newhall, C. G. & Punongbayan, R. S. (eds) *Fire and Mud: Eruptions and Lahars of Mount Pinatubo*. Quezon City: Philippine Institute of Volcanology and Seismology; Seattle, WA: University of Washington Press, pp. 767–798.
- Bourdon, E., Eissen, J. P., Monzier, M., Robin, C., Martin, H., Cotten, J. & Minard, L. H. (2002). Adakite-like lavas from Antisana volcano (Ecuador): evidence for slab melt metasomatism beneath the Andean Northern Volcanic Zone. *Journal of Petrology* **43**, 199–217.

Briaies, A., Patriat, P. & Tapponnier, P. (1993). Updated interpretation of magnetic anomalies and seafloor spreading stages in the South China Sea: implications for the Tertiary tectonics of southeast Asia. *Journal of Geophysical Research* **98**, 6299–6328.

Cardwell, R. K., Isacks, B. L. & Karig, D. E. (1980). The spatial distribution of earthquakes, focal mechanism solutions, and subducted lithosphere in the Philippines and Northeastern Indonesian islands. In: Hayes, D. E. (ed.) *The Tectonic and Geologic Evolution of Southeast Asian Seas and Islands*. *Geophysical Monograph, American Geophysical Union* **23**, 394–396.

Carroll, M. R. & Wyllie, P. J. (1989). Experimental phase relations in the system tonalite–peridotite–H<sub>2</sub>O at 15 kbar: implications for assimilation and differentiation processes near the crust–mantle boundary. *Journal of Petrology* **30**, 1351–1382.

Castillo, P. R. & Punongbayan, R. S. (1996). Petrology and Sr, Nd, and Pb isotopic geochemistry of Mount Pinatubo volcanic rocks. In: Newhall, C. G. & Punongbayan, R. S. (eds) *Fire and Mud: Eruptions and Lahars of Mount Pinatubo*. Quezon City: Philippine Institute of Volcanology and Seismology; Seattle, WA: University of Washington Press, pp. 799–806.

Clynne, M. A. (1999). A complex magma mixing origin for rocks erupted in 1915, Lassen Peak, California. *Journal of Petrology* **40**, 105–132.

Coats, R. R. (1962). Magma type and crustal structure in the Aleutian arc. In: *Crust of the Pacific Basin*. *Geophysical Monograph, American Geophysical Union* **6**, 92–109.

Conrad, W. K., Nicholls, I. A. & Wall, V. J. (1988). Water-saturated and -undersaturated melting of metaluminous and peraluminous crustal compositions at 10 kbar: evidence for the origin of silicic magmas in the Taupo volcanic zone, New Zealand, and other occurrences. *Journal of Petrology* **29**, 765–803.

Costa, F. & Singer, B. (2002). Evolution of Holocene dacite and compositionally zoned magma, Volcán San Pedro, Southern Volcanic Zone, Chile. *Journal of Petrology* **43**, 1571–1593.

Daag, A. S., Dolan, M. T., Laguerta, E. P., Meeker, G. P., Newhall, C. G., Pallister, J. S. & Solidum, R. U. (1996). Growth of a postclimactic lava dome at Mount Pinatubo, July–October 1992. In: Newhall, C. G. & Punongbayan, R. S. (eds) *Fire and Mud: Eruptions and Lahars of Mount Pinatubo*. Quezon City: Philippine Institute of Volcanology and Seismology; Seattle, WA: University of Washington Press, pp. 647–664.

Dall'Agnol, R., Scaillet, B. & Pichavant, M. (1999). An experimental study of a lower Proterozoic A-type granite from the Eastern Amazonian Craton, Brazil. *Journal of Petrology* **40**, 1673–1698.

de Boer, J. Z., Odom, L. A., Ragland, P. C., Snider, F. G. & Tilford, N. R. (1980). The Bataan orogene: eastward subduction, tectonic rotations, and volcanism in the western Pacific (Philippines). *Tectonophysics* **67**, 305–317.

Defant, M. J. & Drummond, M. S. (1990). Derivation of some modern arc magmas by melting of young subducted lithosphere. *Nature* **347**, 662–665.

Defant, M. J., Jacques, D., Maury, R. C. & De Boer, J. Z. (1989). Geochemistry and tectonic setting of the Luzon arc, Philippines. *Geological Society of America Bulletin* **101**, 663–672.

Defant, M. J., Maury, R. C., Ripley, E. M., Feigenson, M. D. & Jacques, D. (1991). An example of island-arc petrogenesis: geochemistry and petrology of the southern Luzon arc, Philippines. *Journal of Petrology* **32**, 455–500.

Delfin, F. G. (1984). Geology and geothermal potential of Mt Pinatubo. Philippine National Oil Company–Energy Development Corporation (PNOC–EDC) internal report, 36 pp.

Delfin, F. G., Villarosa, H. G., Laguyan, D. B., Clemente, V. C., Candelaria, M. R. & Ruaya, J. R. (1996). Geothermal exploration of the pre-1991 Mount Pinatubo hydrothermal system. In: Newhall, C. G. & Punongbayan, R. S. (eds) *Fire and Mud: Eruptions and Lahars of Mount Pinatubo*: Quezon City: Philippine Institute of Volcanology and Seismology; Seattle, WA: University of Washington Press, pp. 197–212.

Devine, J. D., Gardner, J. E., Brach, H. P., Layne, G. D. & Rutherford, M. J. (1995). Comparison of microanalytical methods for estimation of H<sub>2</sub>O contents of silicic volcanic glasses. *American Mineralogist* **73**, 845–849.

Drummond, M. S. & Defant, M. J. (1990). A model for trondhjemite–tonalite–dacite genesis and crustal growth via slab melting: Archaean to modern comparison. *Journal of Geophysical Research* **95**, 21503–21521.

Drummond, M. S., Defant, M. J. & Kepezhinskas, P. K. (1996). Petrogenesis of slab derived-tonalite–dacite adakite magmas. *Transactions of the Royal Society of Edinburgh: Earth Sciences* **87**, 205–215.

Eggler, D. H. (1972). Amphibole stability in H<sub>2</sub>O-undersaturated calc-alkaline melts. *Earth and Planetary Science Letters* **15**, 28–34.

Evans, B. W. & Scaillet, B. (1997). The redox state of Pinatubo dacite and the ilmenite–hematite solvus. *American Mineralogist* **82**, 625–629.

Feeley, T. C. & Hacker, M. D. (1996). Intracrustal derivation of Na-rich andesitic and dacitic magmas: an example from Volcan Ollague, Andean Central Volcanic Zone. *Journal of Geology* **103**, 213–225.

Fogel, R. A. & Rutherford, M. J. (1990). The solubility of carbon dioxide in rhyolitic melts: a quantitative FTIR study. *American Mineralogist* **75**, 1311–1326.

Fournelle, J., Carmody, R. & Daag, A. G. (1996). Mineralogy and geochemistry of Mount Pinatubo anhydrite- and sulfide-bearing pumices from the SO<sub>2</sub>-rich eruption of June (1991). In: Newhall, C. G. & Punongbayan, R. S. (eds) *Fire and Mud: Eruptions and Lahars of Mount Pinatubo*: Quezon City: Philippine Institute of Volcanology and Seismology; Seattle, WA: University of Washington Press, pp. 845–864.

Gerlach, T. M., Westrich, H. R. & Symonds, R. B. (1996). Pre-eruption vapor in magma of the climactic Mount Pinatubo eruption: source of the giant stratospheric sulfur dioxide cloud. In: Newhall, C. G. & Punongbayan, R. S. (eds) *Fire and Mud: Eruptions and Lahars of*

*Mount Pinatubo*. Quezon City: Philippine Institute of Volcanology and Seismology; Seattle, WA: University of Washington Press, pp. 415–434.

Ghiorso, M. S. (1999). On the stability relations of hydrous minerals in water-undersaturated magmas. *American Mineralogist* **84**, 1506–1511.

Gill, J. B. (1981). *Orogenic Andesites and Plate Tectonics*. New York: Springer, 390 pp.

Gill, J. B. & Stork, A. L. (1979). Miocene low-K dacites and trondhjemites of Fiji. In: Barker, F. (ed.) *Trondhjemites, Dacites and Related Rocks*. New York: Elsevier, pp. 629–649.

Green, T. H. (1972). Crystallisation of calc-alkaline andesite under controlled high pressure hydrous conditions. *Contributions to Mineralogy and Petrology* **34**, 150–166.

Green, T. H. (1982). Anatexis of mafic crust and high pressure crystallisation of andesite. In: Thorpe, R. S. (ed.) *Andesite: Orogenic Andesites and Related Rocks*. Chichester: Wiley, pp. 465–487.

Green, T. H. (1992). Experimental phase equilibrium studies of garnet-bearing I-type volcanics and high level intrusives from Northland, New Zealand. *Transactions of the Royal Society of Edinburgh: Earth Sciences* **83**, 429–438.

Green, T. H. & Ringwood, A. E. (1968). Genesis of the calc-alkaline igneous rock suite. *Contributions to Mineralogy and Petrology* **18**, 105–162.

Grove, T. L. & Kinzler, R. L. (1986). Petrogenesis of andesites. *Annual Review of Earth and Planetary Sciences* **14**, 417–454.

Harangi, S. Z., Downes, H., Kosa, L., Szabo, C. S., Thirlwall, M. F., Mason, P. R. D. & Matthey, D. (2001). Almandine garnet in calc-alkaline volcanic rocks of the Northern Pannonian Basin (Eastern–Central Europe): geochemistry, petrogenesis and geodynamic implications. *Journal of Petrology* **42**, 1813–1843.

Hattori, K. (1996). Occurrence and origin of sulfide and sulfate in the 1991 Pinatubo eruption products. In: Newhall, C. G. & Punongbayan, R. S. (eds) *Fire and Mud: Eruptions and Lahars of Mount Pinatubo*. Quezon City: Philippine Institute of Volcanology and Seismology; Seattle, WA: University of Washington Press, pp. 807–824.

Hattori, K. & Sato, H. (1996). Magma evolution recorded in plagioclase zoning in 1991 Pinatubo eruption products. *American Mineralogist* **81**, 982–994.

Helz, R. T. (1982). Phase relations and compositions of amphiboles produced in studies of the melting behavior of rocks. In: Veblen, D. R. & Ribbe, P. H. (eds) *Amphiboles: Petrology and Experimental Phase Relations*. Mineralogical Society of America, *Reviews in Mineralogy* **9**, 279–347.

Hollister, L. S., Grissom, G. C., Peters, E. K., Stowell, H. H. & Sisson, V. V. (1987). Confirmation of the empirical correlation of Al in hornblende with pressure of crystallisation of calc-alkaline plutons. *American Mineralogist* **72**, 231–239.

- Holloway, J. R. (1973). The system pargasite–H<sub>2</sub>O–CO<sub>2</sub>: a model for melting of a hydrous mineral with a mixed volatile fluid—I. Experimental results to 8 kbars. *Geochimica et Cosmochimica Acta* **37**, 651–666.
- Holtz, F., Pichavant, M., Barbey, P. & Johannes, W. (1992). Effects of H<sub>2</sub>O on liquidus phase relations in the haplogranite system at 2 and 5 kbar. *American Mineralogist* **77**, 1223–1241.
- Imai, A., Listanco, E. L. & Fujii, T. (1996). Highly oxidized and sulfur-rich dacitic magma of Mount Pinatubo: implication for metallogenesis of porphyry copper mineralization in the Western Luzon arc. In: Newhall, C. G. & Punongbayan, R. S. (eds) *Fire and Mud: Eruptions and Lahars of Mount Pinatubo*. Quezon City: Philippine Institute of Volcanology and Seismology; Seattle, WA: University of Washington Press, pp. 865–974.
- Johnson, M. C. & Rutherford, M. J. (1989). Experimental calibration of the aluminium-in-hornblende geobarometer with application to Long Valley caldera (California) volcanic rocks. *Geology* **17**, 837–841.
- Kay, R. W. (1978). Aleutian magnesian andesites: melts from subducted Pacific ocean crust. *Journal of Volcanology and Geothermal Research* **4**, 497–522.
- Kay, S. M., Ramos, V. A. & Marquez, M. (1993). Evidence in Cerro Pampa volcanic rocks for slab melting prior to ridge– trench collision in Southern South America. *Journal of Geology* **101**, 703–714.
- Kepezhinskas, P. K., Defant, M. J. & Drummond, M. S. (1995). Na-metasomatism in the island-arc mantle by slab melt–peridotite interactions: evidence from mantle xenoliths in the north Kamchatka arc. *Journal of Petrology* **36**, 1505–1527.
- Kushiro, I. (1972). Effect of water on the composition of magmas formed at high pressure. *Journal of Petrology* **13**, 311–334.
- Leake, B. E., Woolley, A. R., Arps, C. E. S., *et al.* (1997). Nomenclature of amphiboles: report of the subcommittee on amphiboles of the international mineralogical association commission on the new minerals and mineral names. *Mineralogical Magazine* **61**, 295–321.
- Listanco, E. L., Yumul, G. P., Jr & Datuin, R. T. (1997). On the thickness of the Philippine crust: application of the Plank–Langmuir systematics. *Journal of the Geological Society of the Philippines* **52**, 20–24.
- Luhr, J. F. & Melson, W. G. (1996). Mineral and glass compositions in June 15, 1991, pumices: evidence for dynamic disequilibrium in the Pinatubo dacite. In: Newhall, C. G. & Punongbayan, R. S. (eds) *Fire and Mud: Eruptions and Lahars of Mount Pinatubo*. Quezon City: Philippine Institute of Volcanology and Seismology; Seattle, WA: University of Washington Press, pp. 733–750.
- Martel, C., Pichavant, M., Bourdier, J. L., Traineau, H., Holz, F. & Scaillet, B. (1998). Magma storage conditions and control of eruption regime in silicic volcanoes: experimental evidence from Mt. Pelée. *Earth and Planetary Science Letters* **156**, 89–99.

- Miyashiro, A. (1974). Volcanic rock series in island arcs and active continental margins. *American Journal of Science* **274**, 321–355.
- Mooney, W. D., Laske, G. & Guy Masters, T. (1998). CRUST 5.1. A global crustal model at 5° 5°. *Journal of Geophysical Research* **103**, 727–747.
- Mori, J., Eberhart-Phillips, D. & Harlow, D. H. (1996). Three dimensional velocity structure at Mount Pinatubo, Philippines: resolving magma bodies and earthquakes hypocenters. In: Newhall, C. G. & Punongbayan, R. S. (eds) *Fire and Mud: Eruptions and Lahars of Mount Pinatubo*. Quezon City: Philippine Institute of Volcanology and Seismology; Seattle, WA: University of Washington Press, pp. 371–382.
- Müntener, O., Kelemen, P. & Grove, T. L. (2001). The role of H<sub>2</sub>O during crystallisation of primitive arc magmas under uppermost mantle conditions and genesis of igneous pyroxenites: an experimental study. *Contributions to Mineralogy and Petrology* **141**, 643–658.
- Mysen, B. O. & Boettcher, A. L. (1975). Melting of a hydrous mantle. II. Geochemistry of crystals and liquids formed by anatexis of mantle peridotite at high pressures and high temperatures as a function of controlled activities of water, hydrogen, and carbon dioxide. *Journal of Petrology* **16**, 549–593.
- Naney, M. T. (1983). Phase equilibria of rock-forming ferromagnesian silicates in granitic systems. *American Journal of Science* **283**, 993–1033.
- Newhall, C. G., Daag, A. S., Delfin, F. G., Hoblitt, R. P., McGeehin, J., Pallister, J. S., Regalado, M. T. M., Rubin, M., Tubianosa, B. S., Tamayo, R. A. & Umbal, J. V. (1996). Eruptive history of Mount Pinatubo. In: Newhall, C. G. & Punongbayan, R. S. (eds) *Fire and Mud: Eruptions and Lahars of Mount Pinatubo*. Quezon City: Philippine Institute of Volcanology and Seismology; Seattle, WA: University of Washington Press, pp. 165–195.
- Nicholls, I. & Ringwood, A. E. (1973). Effect of water on olivine stability in tholeiites and production of silica-saturated magmas in the island arc environment. *Journal of Geology* **81**, 285–300.
- Nixon, G. T. (1988). Petrology of the younger andesites and dacites of Iztaccihuatl volcano, Mexico: I. Disequilibrium phenocryst assemblages as indicators of magma chamber processes. *Journal of Petrology* **29**, 213–264.
- Pallister, J. S., Hoblitt, R. P., Meeker, G. P., Knight, R. J. & Siems, D. F. (1996). Magma mixing at Mount Pinatubo: petrographic and chemical evidence from 1991 deposits. In: Newhall, C. G. & Punongbayan, R. S. (eds) *Fire and Mud. Eruptions and Lahars of Mount Pinatubo*. Quezon City: Philippine Institute of Volcanology and Seismology; Seattle, WA: University of Washington Press, pp. 687–732.
- Peacock, S. M., Rushmer, T. & Thompson, A. B. (1994). Partial melting of subducting oceanic crust. *Earth and Planetary Science Letters* **121**, 227–244.
- Petford, N. & Atherton, M. (1996). Na-rich partial melts from newly underplated basaltic crust: the Cordillera Blanca batholith, Peru. *Journal of Petrology* **37**, 1491–1521.

- Pichavant, M. (1987). Effects of B and H<sub>2</sub>O on liquidus phase relations in the haplogranite system at 1 kbar. *American Mineralogist* **72**, 1056–1070.
- Pichavant, M., Martel, C., Bourdier, J. L. & Scaillet, B. (2002a). Physical conditions, structure and dynamics of a zoned magma chamber: Mt. Pelée (Martinique, Lesser Antilles Arc). *Journal of Geophysical Research* **107**(B5), 10.1029/2001JB000315.
- Pichavant, M., Mysen, B. O. & Macdonald, R. (2002b). Source and H<sub>2</sub>O content of high-MgO magmas in island arc settings: an experimental study of a primitive calc-alkaline basalt from St. Vincent, Lesser Antilles arc. *Geochimica et Cosmochimica Acta* **66**, 2193–2209.
- Pownceby, M. I. & O'Neill, H. St. C. (1994). Thermodynamic data from redox reactions at high temperatures. III. Activity–composition relations in Ni–Pd alloys from EMF measurements at 850–1250 K, and calibration of the NiO + Ni–Pd assemblage as a redox sensor. *Contributions to Mineralogy and Petrology* **116**, 327–339.
- Prouteau, G., Scaillet B., Pichavant, M. & Maury, R. C. (1999). Fluid-present melting of ocean crust in subduction zones. *Geology* **27**, 1111–1114.
- Prouteau, G., Scaillet, B., Pichavant, M. & Maury, R. C. (2001). Evidence of mantle metasomatism by hydrous silicic melts derived from subducted oceanic crust. *Nature* **410**, 197–200.
- Rapp, R. P. & Watson, E. B. (1995). Dehydration melting of metabasalt at 8–32 kbar: implications for continental growth and crust–mantle recycling. *Journal of Petrology* **36**, 891–931.
- Rapp, R. P., Watson, E. B. & Miller, C. F. (1991). Partial melting of amphibolite/eclogite and origin of Archean trondhjemites and tonalites. *Precambrian Research* **51**, 1–25.
- Rapp, R. P., Shimizu, N., Norman, M. D. & Applegate, G. S. (1999). Reaction between slab-derived melts and peridotite in the mantle wedge: experimental constraints at 3–8 GPa. *Chemical Geology* **160**, 335–356.
- Richard, M., Bellon, H., Maury, R., Barrier, E. & Juang, W. S. (1986). Miocene to recent calc-alkalic volcanism in eastern Taiwan: K–Ar ages and petrography. *Tectonophysics* **125**, 87–102.
- Roux, J. & Lefèvre, A. (1992). A fast quench device for internally heated pressure vessels. *European Journal of Mineralogy* **4**, 279–281.
- Rutherford, M. J. & Devine, J. D. (1996). Pre-eruption pressure–temperature conditions and volatiles in the 1991 Mount Pinatubo magma. In: Newhall, C. G. & Punongbayan, R. S. (eds) *Fire and Mud: Eruptions and Lahars of Mount Pinatubo*. Quezon City: Philippine Institute of Volcanology and Seismology; Seattle, WA: University of Washington Press, pp. 751–766.
- Scaillet, B. & Evans, B. W. (1999). The June 15, 1991, eruption of Mount Pinatubo: I. Phase equilibria and pre-eruption  $P$ – $T$ – $f_{O_2}$ – $f_{H_2O}$  conditions of the dacite magma. *Journal of Petrology* **40**, 381–411.

- Scaillet, B., Pichavant, M. & Roux, J. (1995).** Experimental crystallization of leucogranite magmas. *Journal of Petrology* **36**, 663–705.
- Schmidt, M. W. (1992). Amphibole composition in tonalite as a function of pressure: an experimental calibration of the Al-in-hornblende barometer. *Contributions to Mineralogy and Petrology* **110**, 304–310.
- Sen, S. & Dunn, T. (1994a). Dehydration melting of a basaltic composition amphibolite at 1.5 and 2.0 GPa: implications for the origin of adakites. *Contributions to Mineralogy and Petrology* **117**, 394–409.
- Sen, S. & Dunn, T. (1994b). Experimental modal metasomatism of a spinel lherzolite and the production of amphibole-bearing peridotite. *Contributions to Mineralogy and Petrology* **119**, 422–432.
- Silver, L. A., Ihinger, P. D. & Stolper, E. M. (1990). The influence of bulk composition on the speciation of water in silicate glasses. *Contributions to Mineralogy and Petrology* **104**, 142–162.
- Singer, B. S., Myers, J. D. & Frost, C. D. (1992). Mid-Pleistocene lavas from the Segum volcanic center, central Aleutian arc: closed-system fractional crystallization of a basalt to rhyodacite eruptive suite. *Contributions to Mineralogy and Petrology* **110**, 87–112.
- Sisson, T. W. & Grove, T. L. (1993). Experimental investigations of the role of water in calc-alkaline differentiation and subduction zone magmatism. *Contributions to Mineralogy and Petrology* **113**, 143–166.
- Smith, D. R. & Leeman, W. P. (1987). Petrogenesis of Mount St. Helens dacitic magmas. *Journal of Geophysical Research* **92**, 10313–10334.
- Springer, W. & Seck, H. A. (1997). Partial fusion of basic granulites at 5 to 15 kbar: implications for the origin of TTG magmas. *Contributions to Mineralogy and Petrology* **127**, 30–45.
- Stern, C. R. & Kilian, R. (1996). Role of subducted slab, mantle wedge and continental crust in the generation of adakites from the Andean Austral Volcanic Zone. *Contributions to Mineralogy and Petrology* **123**, 263–281.
- Stormer, J. C. (1983). The effects of recalculation on estimates of temperature and oxygen fugacity from analyses of multi-component iron–titanium oxides. *American Mineralogist* **68**, 586–594.
- Taylor, J. R., Wall, V. J. & Pownceby, M. I. (1992). The calibration and application of accurate sensors. *American Mineralogist* **77**, 284–295.
- Tomblin, J. F. (1979). Dacite of the lesser Antilles. In: Barker, F. (ed.) *Trondhjemites, Dacites and Related Rocks*. New York: Elsevier, pp. 601–628.

Van der Laan, S. R. & Wyllie, P. J. (1992). Constraints on Archean trondhjemite genesis from hydrous crystallisation experiments on Nûk gneiss at 10–17 kbar. *Journal of Geology* **100**, 57–68.

Wareham, C. D., Millar, I. L. & Vaughan, A. P. M. (1997). The generation of sodic granite magmas, western Palmer Land, Antarctic Peninsula. *Contributions to Mineralogy and Petrology* **128**, 81–96.

Westrich, H. R. & Gerlach, T. M. (1992). Magmatic gas source for the stratospheric SO<sub>2</sub> cloud from the June 15, 1991 eruption of Mount Pinatubo. *Geology* **20**, 867–870.

Winther, K. T. & Newton, R. C. (1991). Experimental melting of hydrous low-K tholeiite: evidence on the origin of Archean cratons. *Bulletin of the Geological Society of Denmark* **39**, 213–228.

Wolf, M. B. & Wyllie, P. J. (1994). Dehydration melting of amphibolite at 10 kbar: the effect of temperature and time. *Contributions to Mineralogy and Petrology* **115**, 369–383.

Wu, F. T. (1979). Recent tectonics in Taiwan. In: Uyeda, S., Murphy, S. W. & Kobayashi, K. (eds) *Geodynamics of the Western Pacific*. Japan Scientific Society Press, pp. 265–299.

## FIGURES

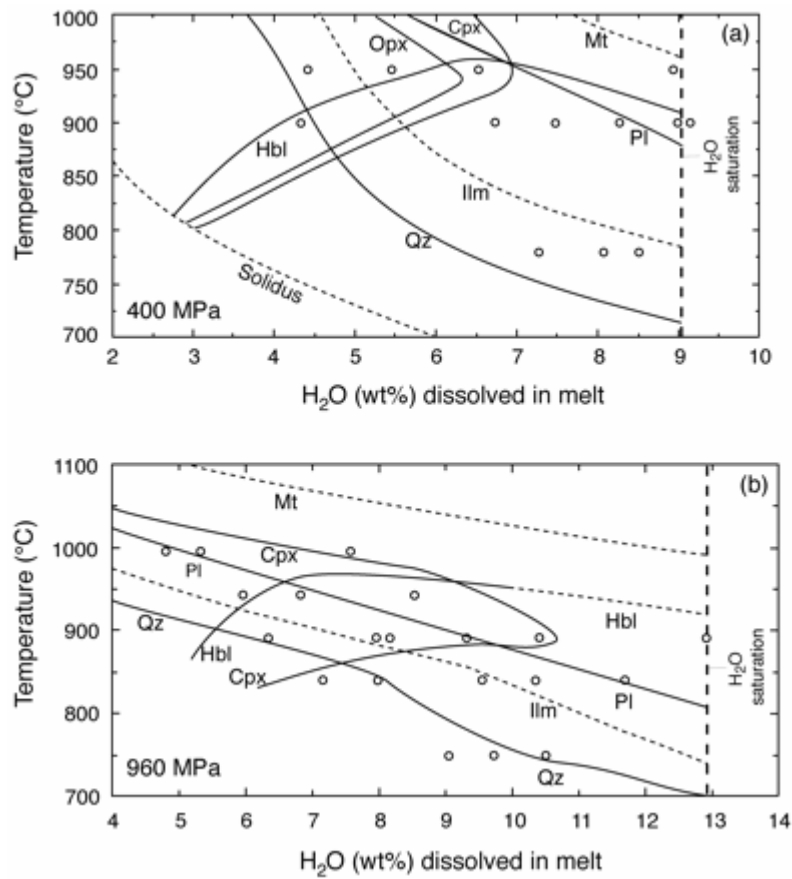


**Fig. 1.** Isobaric phase relationships of the Pinatubo dacite at 400 and 960 MPa. The wt % H<sub>2</sub>O axis is the amount of dissolved water in the melt. Cpx, clinopyroxene; Opx, orthopyroxene; Hbl, hornblende; Pl, plagioclase; Qz, quartz; Ilm, ilmenite; Mt, magnetite. The experiments at 780°C and 400 MPa are from Scaillet & Evans (1999). Dashed lines are for inferred (ilmenite, solidus) or extrapolated (hornblende) stability curves.

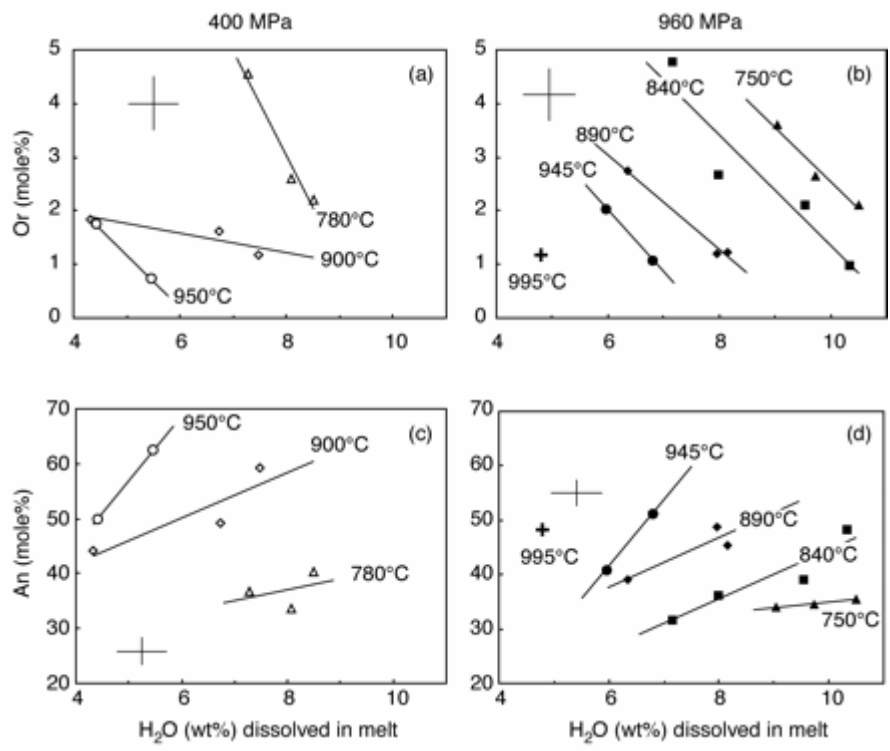
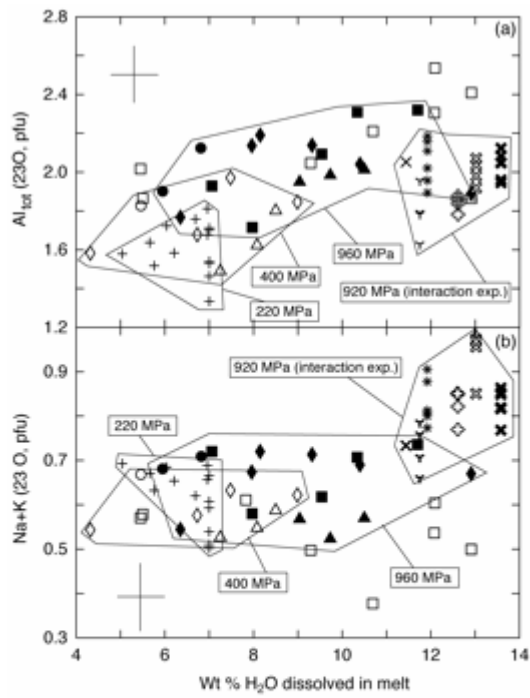


**Fig. 2.** Variation of plagioclase composition with changes in melt water content and temperature at 400 MPa (a and c), and 960 MPa (b and d). The vertical bar is the average standard deviation and the horizontal bar is the maximum uncertainty on melt water content.



+ 220 MPa, Scaillet & Evans, 1999

△ 780°C

◇ 900°C

○ 950°C

▲ 750°C

■ 840°C

◆ 890°C

● 945°C

□ Tsupo dache, 1000 MPa, Conrad et al., 1988

920 MPa interaction experiments :

● As10

× As11

▽ As12

◆ As26

× As27

◇ As28

950°C

1000°C

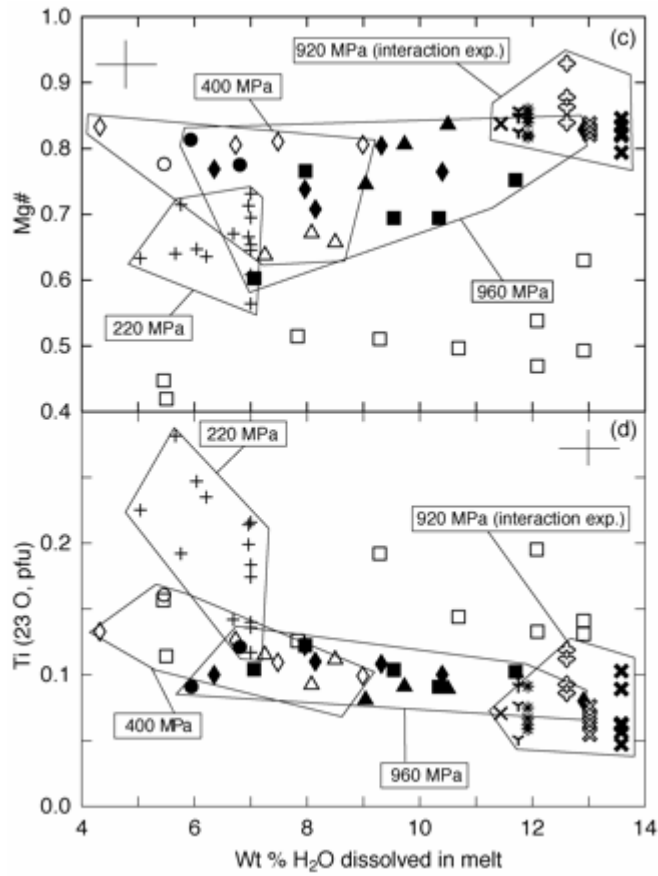


**Fig. 3.** Variation of amphibole composition (atoms p.f.u.) with changes in melt water content at various temperatures and pressures. The vertical bar is the average standard deviation and the horizontal bar is the maximum uncertainty on melt water content. Mg number =  $Mg/(Mg + Fe_{tot})$ .

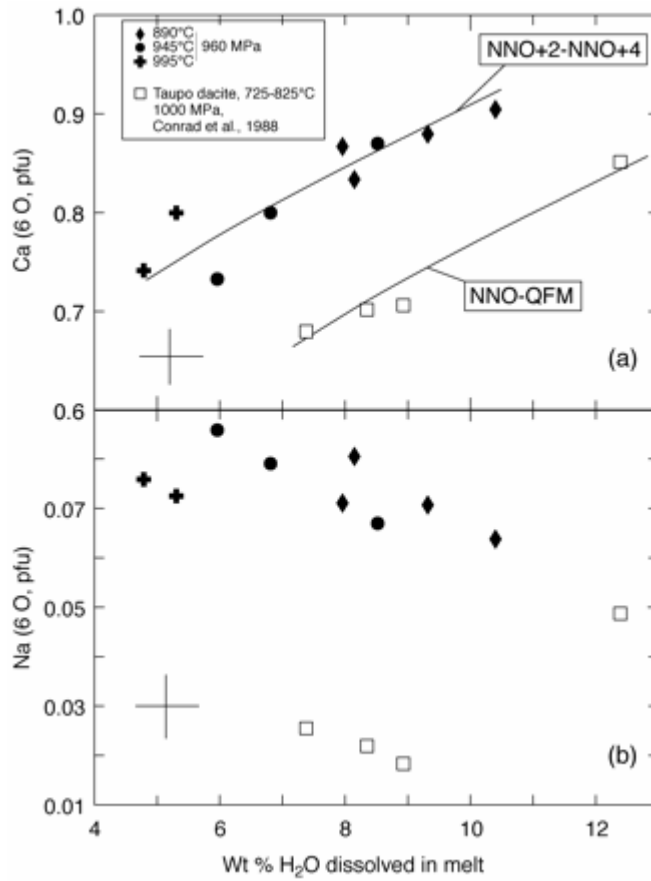
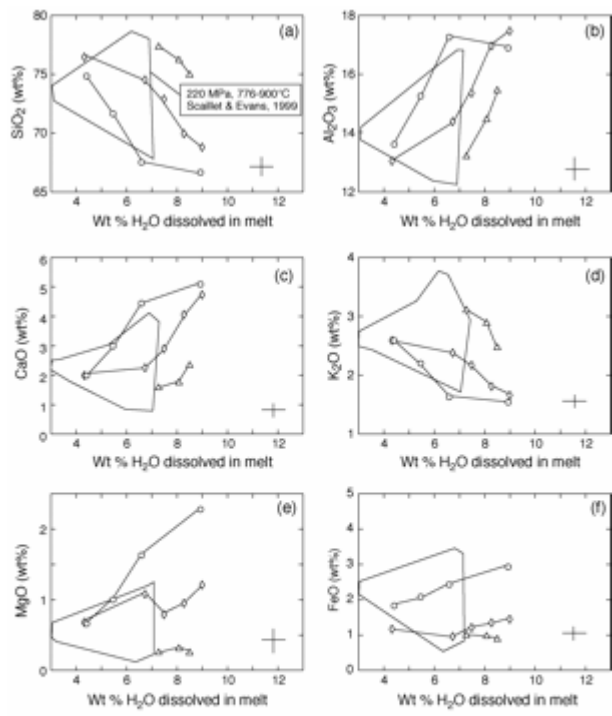


**Fig. 4.** Variation of clinopyroxene composition (atoms p.f.u.) with changes in melt water content at different temperatures at 960 MPa. The vertical bar is the average standard deviation and the horizontal bar is the maximum uncertainty on melt water content.



- |  |   |
|--|---|
| <ul style="list-style-type: none"> <li>△ 780°C</li> <li>○ 900°C</li> <li>○ 950°C</li> <li>▲ 750°C</li> <li>■ 940°C</li> <li>● 890°C</li> <li>● 945°C</li> <li>● 950°C</li> <li>□ Tsupo dactile, 1000 MPa, Conrad et al., 1988</li> </ul> | <p><b>920 MPa interaction experiments:</b></p> <ul style="list-style-type: none"> <li>■ As10</li> <li>× As11</li> <li>▼ As12</li> <li>⊞ As26</li> <li>× As27</li> <li>◇ As28</li> </ul> |
|--|---|
- 950°C
- 1000°C

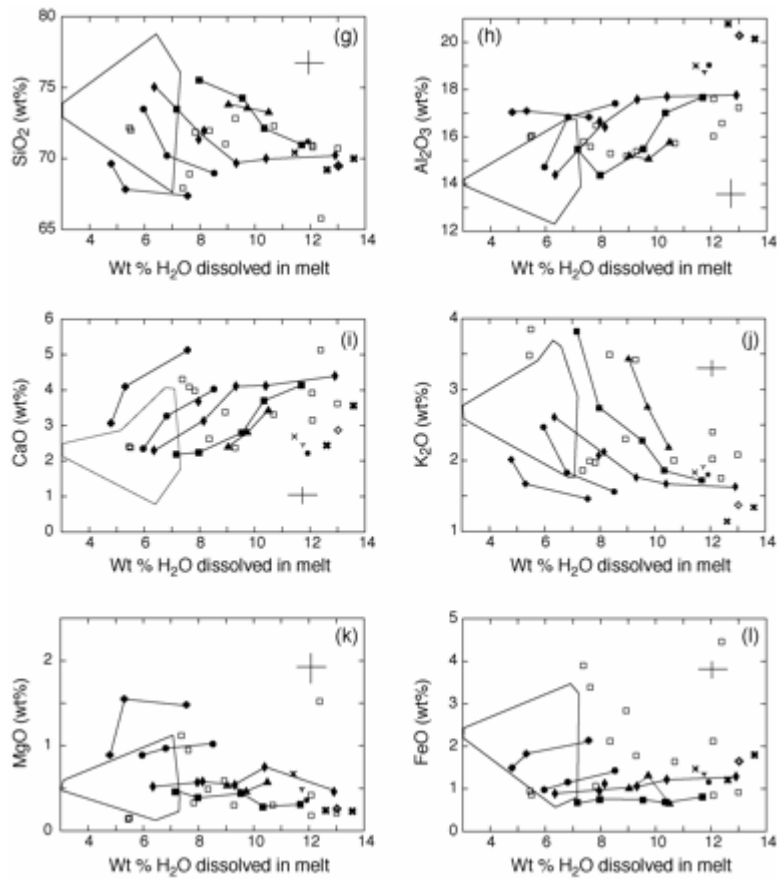


**Fig. 5.** Variation of melt composition (recalculated to 100 wt % volatile free) with changes in melt water content and temperature at 400 MPa (a–f), and 960 MPa (g–l). The vertical bar is the average standard deviation and the horizontal bar is the maximum uncertainty on melt water content. The 220 MPa data are from Scaillet & Evans (1999). The experimental melts of Conrad *et al.* (1988) are also shown for comparison.

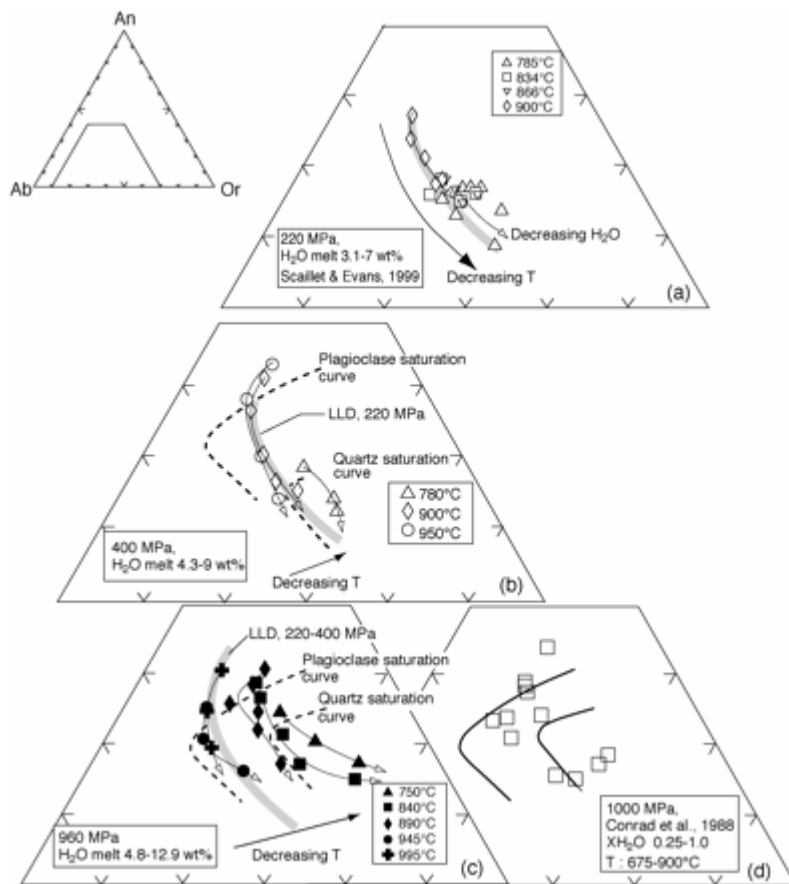


**Fig. 6.** Experimental melt compositions in term of CIPW normative albite (Ab), anorthite (An) and orthoclase (Or). At 220 MPa (Scaillet & Evans, 1999), all melts are saturated in plagioclase. The experimental melts of Conrad *et al.* (1988) are also shown for comparison. LLD, liquid line of descent. On the 400 and 960 MPa ternary diagrams, melts saturated with plagioclase and plagioclase + quartz lie below, or to the right of the two saturation curves shown. The open arrows indicate the effect of decreasing melt water content on melt composition at constant temperature (i.e. an increase in crystallization), whereas the black arrow indicates the effect of falling temperature.

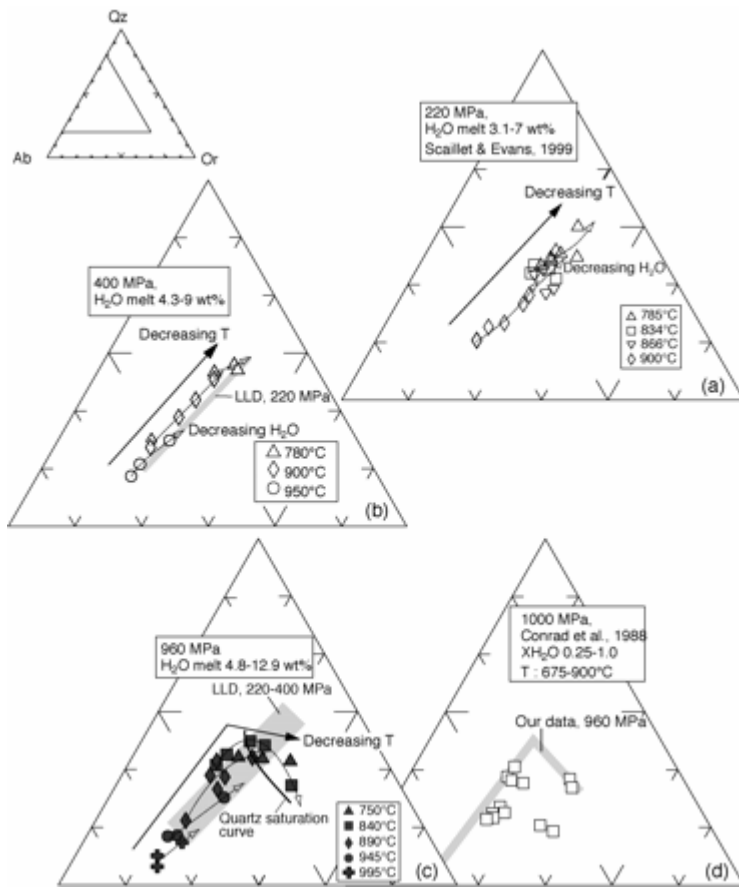


**Fig. 7.** Experimental melt compositions in term of CIPW normative albite (Ab), quartz (Qz) and orthoclase (Or). The experimental melts of Conrad *et al.* (1988) are also shown for comparison. LLD, liquid line of descent. The open arrows indicate the effect of decreasing melt water content on melt composition at constant temperature (i.e. an increase in crystallization), whereas the black arrow indicates the effect of falling temperature.

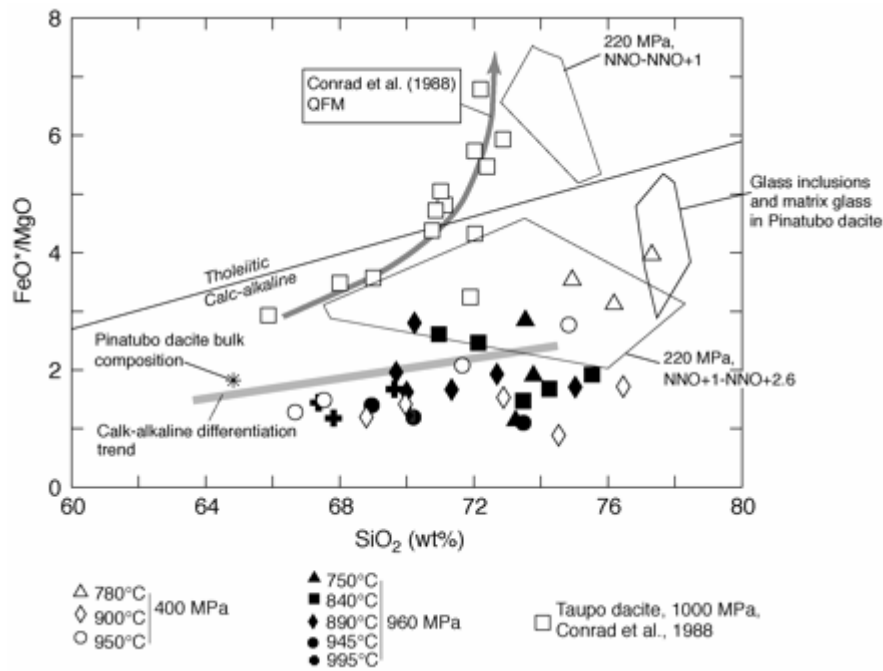


**Fig. 8.** Experimental melts plotted on an  $\text{FeO}^*/\text{MgO}$  vs  $\text{SiO}_2$  variation diagram. The tholeiitic–calc-alkaline divide line is from Miyashiro (1974). The calc-alkaline differentiation trend is after Grove & Kinzler (1986). The compositions of the Pinatubo dacite (Pallister *et al.*, 1996), glass inclusions and matrix glass in the dacite (Gerlach *et al.*, 1996; Rutherford & Devine, 1996) are also reported. The fields labelled 220 MPa delineate the melt compositions produced from dacite crystallization at 220 MPa under either high (NNO + 1 to NNO + 2.6) or moderate (NNO to NNO + 1)  $f_{\text{O}_2}$  (Scaillet & Evans, 1999). The experimental melts of Conrad *et al.* (1988) are also shown for comparison.

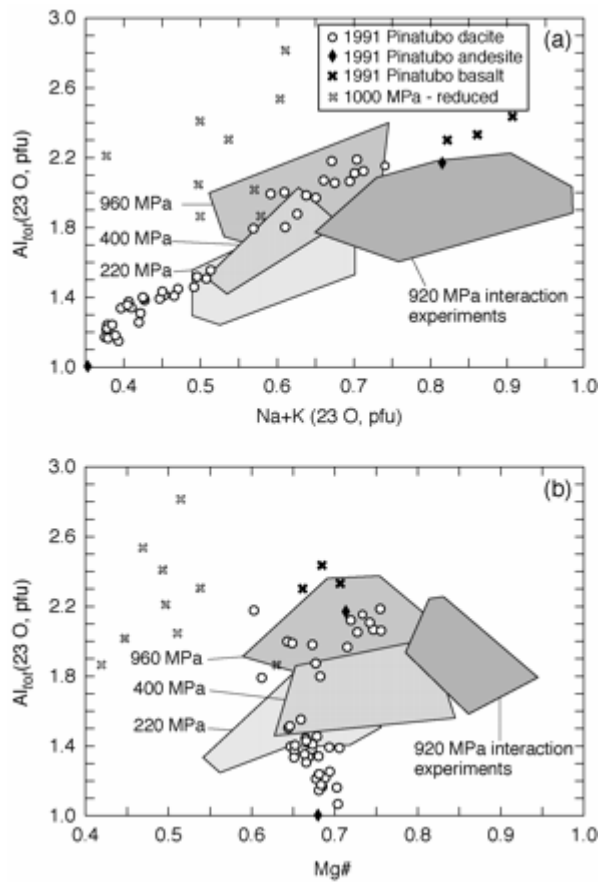


**Fig. 9.** Amphiboles in the 1991 Pinatubo dacite (Bernard *et al.*, 1991, 1996), andesite (Bernard *et al.*, 1996) and basalt (Bernard *et al.*, 1996; Pallister *et al.*, 1996) compared with experimental amphiboles produced in the dacite system at 220 MPa (Scaillet & Evans, 1999), 400 and 960 MPa (this work). The compositions of amphiboles produced at 1000 MPa and low  $f_{O_2}$  (1000 MPa-reduced) (Conrad *et al.*, 1988) are also shown for comparison.

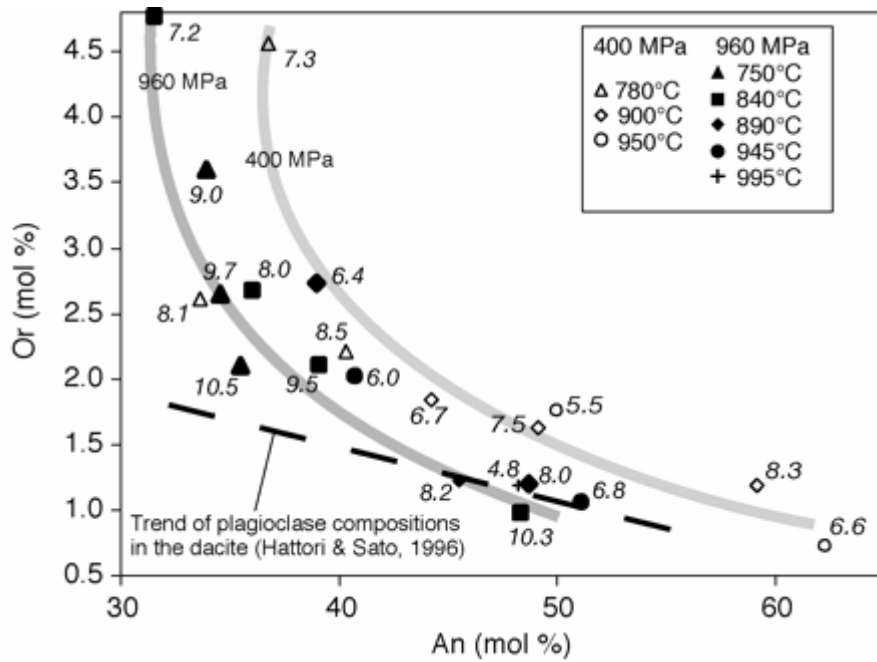


**Fig. 10.** Comparison of the Pinatubo dacite plagioclase Or–An compositions (Hattori & Sato, 1996) with experimental plagioclase produced at 400 and 960 MPa; numbers in italics indicate the water content (wt %) of the coexisting melt. The thick grey lines show the trends of plagioclase composition with increase in crystallization at either 400 or 960 MPa.

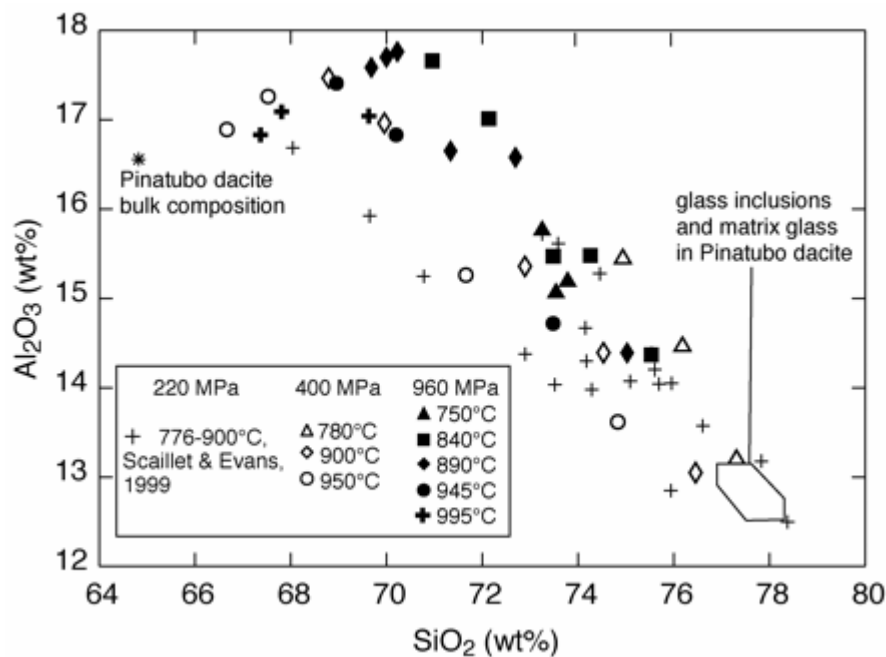


**Fig. 11.** Variation of  $\text{Al}_2\text{O}_3$  vs  $\text{SiO}_2$  contents of mineral glass inclusions in phenocrysts (plagioclase, quartz, amphiboles) and matrix glasses from the Pinatubo dacite (Gerlach *et al.*, 1996) and of experimental glasses [this study and Scaillet & Evans (1999)].

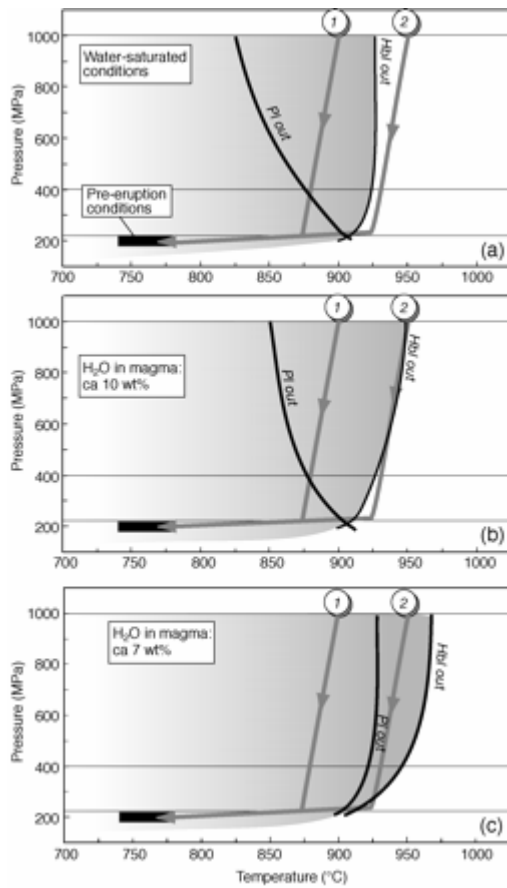


**Fig. 12.** Possible ascent paths for the Pinatubo dacite, calculated assuming production and/or storage of the dacite magma at 1000 MPa followed by near-adiabatic ascent to depth equivalent to 200 MPa. In each panel two ascent trajectories, corresponding to starting temperatures of 900°C (curve labelled 1) and 950°C (curve labelled 2), are shown. The hornblende (Hbl out) and plagioclase (Pl out) liquidus curves are shown for (a) a water-saturated magma, (b) a magma with 10 wt % H<sub>2</sub>O, and (c) a magma with 7 wt % H<sub>2</sub>O. The liquidus curves have been drawn using the experimental constraints of this study and those of Rutherford & Devine (1996) and Scaillet & Evans (1999). (See text for additional details.)

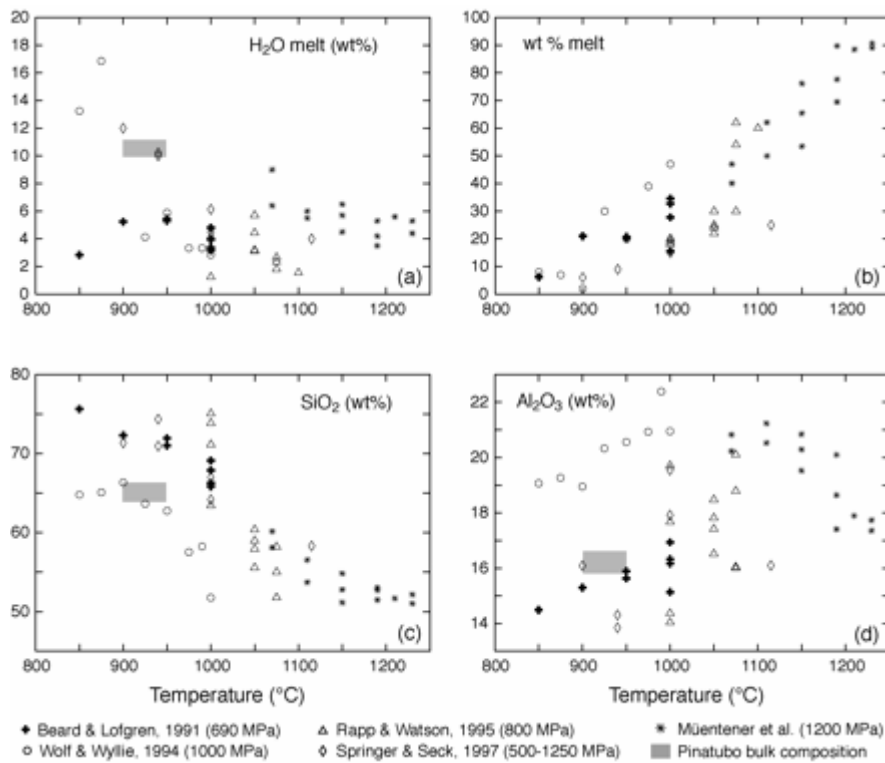


**Fig. 13.** Comparison between the compositions of experimental melts obtained in representative dehydration melting studies of metabasalts performed at mid- to lower-crustal pressures (Beard & Lofgren, 1991; Wolf & Wyllie, 1994; Rapp & Watson, 1995; Springer & Seck, 1997) and the composition of Pinatubo dacite, including its water content. The water content of experimental melts has been estimated using the modal composition of the run products when available, or the difference from 100% of hydrous glass analyses. Also shown are the experimental melts obtained by equilibrium crystallization of primitive arc magmas at upper-mantle conditions (Muentener *et al.*, 2001). The grey box represents the bulk composition of the Pinatubo dacite and the  $T$ - $H_2O_{\text{melt}}$  conditions of its production, as inferred in the present study. It should be noted that none of the dehydration melting experiments reproduce the Pinatubo dacite under  $T$ - $H_2O_{\text{melt}}$  conditions relevant to its fabrication.

## TABLES

Table 1: Compositions of the Pinatubo dacite, average Cenozoic adakites and other dacites used in experimental studies\*

	Pinatubo, 1991	Adakites, Cenozoic	Mount St. Helens, 1980	Taupo-1* greywacke	Taupo-2* dacite	Taipa* dacite
<i>wt %</i>						
SiO <sub>2</sub>	64.6	63.9	62.6	65.0	65.2	64.76
Al <sub>2</sub> O <sub>3</sub>	16.5	17.4	17.8	16.5	15.7	16.93
TiO <sub>2</sub>	0.53	0.61	0.68	0.73	0.60	0.53
FeO <sub>tot</sub>	4.37	4.21	5.14	7.0	5.0	4.64
MgO	2.39	2.47	2.22	1.9	2.5	2.01
CaO	5.23	5.23	5.35	3.5	5.3	5.14
Na <sub>2</sub> O	4.49	4.40	4.48	3.4	3.6	3.51
K <sub>2</sub> O	1.54	1.52	1.29	1.9	1.7	2.25
<i>ppm</i>						
Cr	37.3	54	—	—	—	—
Ni	16.4	39	—	—	—	—
Sr	581	869	463	—	—	—
Y	—	9.5	—	—	—	—
Yb	1.2	0.91	—	—	—	—
La	15.9	17.55	12	—	—	—

Bulk-rock or starting material analyses for experiments(\*) are from: Pinatubo: Pallister *et al.* (1996); adakites: Drummond *et al.* (1996); Mount St. Helens: Smith & Leeman (1987);  
\*Taupo: Conrad *et al.* (1988); \*Taipa: Green (1992).

Table 2: Experimental conditions, run products and phase proportions

Run no.	H <sub>2</sub> O <sub>melt</sub> * (wt %)	$\Delta$ NNO <sup>†</sup>	Run products and phase proportions (wt %)	$\Sigma r^2$
<i>P: 400 MPa; T: 900°C; run duration: 121 h</i>				
PIN86s <sup>‡</sup>	9.0	+4.0	Gl (91.7), Hbl (5.1), Tmg (3.2)	0.33
PIN87s	8.3	+3.8	Gl (86.4), Hbl (7.4), Tmg (3.5), Pl (2.7)	0.07
PIN88s	7.5	+3.6	Gl (71.1), Pl (17.1), Hbl (8.3), Tmg (3.6)	0.12
PIN89s	6.7	+3.4	Gl (62.1), Pl (26.4), Hbl (7.6), Tmg (3.9)	0.20
PIN91s	4.3	+3.0	Gl (59.7), Pl (29.9), Hbl (8.6), Tmt (3.7), Q (tr)	0.15
PIN92s	—	—	Gl, Opx, Cpx, Pl, Q, Tmg	
PIN93s	—	—	Gl, Opx, Cpx, Pl, Q, Tmg	
<i>P: 400 MPa; T: 950°C; run duration: 63 h</i>				
PIN96s	8.9	+4.0	Gl (98.3), Tmg (1.8)	0.28
PIN97s	6.6	+3.5	Gl (94.9), Cpx (4.1), Tmt (2.4), Pl (tr), Hbl (tr),	0.03
PIN98s	5.5	+3.2	Gl (70.3), Pl (20.7), Cpx (3.2), Tmt (3.0), Opx (2.9)	0.03
PIN99s	4.4	+3.0	Gl (58.4), Pl (31.8), Opx (4.2), Cpx (2.2), Tmt (3.4)	0.09
<i>P: 940 MPa; T: 750°C; run duration: 309 h</i>				
PIN100	10.5	+4.8	Gl (68.4), Pl (18.3), Hbl (9.4), Tmg (3.9), Hilm (tr)	0.11
PIN99	9.7	+4.7	Gl (53.1), Pl (29.3), Hbl (10.5), Qtz (3.8), Tmg (3.3)	0.07
PIN98	9.0	+4.6	Gl (39.4), Pl (38.7), Hbl (10.5), Qtz (8.4), Tmg (3.0)	0.08
<i>P: 960 MPa; T: 841°C; run duration: 144 h</i>				
PIN106	11.7	+2.9	Gl (85.7), Hbl (11.0), Tmg (3.3)	0.69
PIN105	10.3	+2.7	Gl (81.3), Hbl (12.6), Pl (2.9), Tmg (3.1)	0.75
PIN104	9.5	+2.6	Gl (64.9), Pl (19.8), Hbl (11.7), Tmg (3.3), Qtz (tr), Hilm (tr)	0.32
PIN103	8.0	+2.3	Gl (53.2), Pl (32.2), Hbl (9.5), Tmg (3.4), Qtz (1.7)	0.06
PIN102	7.2	+2.1	Gl (31.3), Pl (41.6), Hbl (12.6), Qtz (10.9), Tmg (3.6)	0.03

P: 830 MPa; T: 892°C; run duration: 143 h

PIN88	9.3	+2.6	Gl (86.9), Hbl (8.1), Tmg (3.6), Cpx (1.4)	0.40
PIN87	8.0	+2.4	Gl (80.2), Hbl (9.1), Pl (6.4), Tmg (3.4), Cpx (0.9)	0.13
PIN86	6.4	+2.0	Gl (57.7), Pl (28.9), Hbl (9.6), Tmg (3.7)	0.12

P: 970 MPa; T: 892°C; run duration: 146 h

PIN110 <sup>†</sup>	12.9	+3.0	Gl (87.5), Hbl (9.2), Tmg (3.3)	0.85
PIN109	10.4	+2.7	Gl (88.0), Hbl (6.5), Tmg (3.4), Cpx (2.1)	0.47
PIN108	8.2	+2.4	Gl (76.4), Pl (9.5), Hbl (7.8), Cpx (3.2), Tmg (3.0)	0.15

P: 960 MPa; T: 943°C; run duration: 125 h

PIN92	8.5	+3.4	Gl (89.6), Cpx (3.6), Hbl (3.4), Tmg (3.4)	0.37
PIN91	6.8	+3.0	Gl (83.4), Cpx (6.5), Pl (4.9), Tmg (3.3), Hbl (1.9)	0.32
PIN90	6.0	+2.6	Gl (63.2), Cpx (8.4), Pl (24.4), Tmg (4.0)	0.32

P: 980 MPa; T: 995°C; run duration: 50 h

PIN96	7.6	+3.7	Gl (97.2), Tmg (2.8)	0.80
PIN95	5.3	+2.7	Gl (92.3), Cpx (4.7), Tmg (3.0)	0.90
PIN94	4.8	+2.2	Gl (82.2), Cpx (9.6), Pl (5.3), Tmg (2.8)	0.52

Phase proportions calculated using a least-square mass balance (Albarède, 1995). Phase abbreviations: Gl, glass; Pl, plagioclase; Qtz, quartz; Hbl, hornblende; Cpx, clinopyroxene; Opx, orthopyroxene; Tmg, titanomagnetite; Hilm, hemoilmenite.

\* Determined by using the by-difference method.

<sup>†</sup> Estimated error on  $f_{O_2}$  is 0.5 log unit.

<sup>‡</sup> Water-saturated runs.

Table 3: Experimental conditions and run products for interaction experiments

Run no.	H <sub>2</sub> O* (wt %)	Dacite <sup>†</sup> (wt %)	Ultramafic mixture			Run products
			Ol (wt %)	Opx (wt %)	Cpx (wt %)	
<i>P: 920 MPa; T: 950°C; run duration: 95 h</i>						
As10	11.9	57.8	100	—	—	Gl, Ol, Opx1, Opx2, Hbl, Phl
As11	11.4	57.8	79.5	20.5	—	Gl, Ol, Opx1, Opx2, Hbl
As12	11.8	57.5	79.7	15	5.3	Gl, Ol, Opx1, Opx2, Cpx, Hbl
<i>P: 920 MPa; T: 1000°C; run duration : 94 h</i>						
As26	12.6	57.4	100.0	—	—	Gl, Ol, Opx1, Opx2, Hbl
As27	13.4	59.4	78.7	21.3	—	Gl, Ol, Opx1, Opx2, Hbl
As28	13.0	57.7	79.7	15.1	5.3	Gl, Ol, Opx1, Opx2, Cpx, Hbl

Phase abbreviations: Gl, glass; Ol, olivine; Opx, orthopyroxene; Cpx, clinopyroxene; Hbl, hornblende; Phl, phlogopite. Opx1 and Opx2 refer to the starting and newly grown orthopyroxene, respectively.

\* H<sub>2</sub>O in glass as determined by the by-difference method.

<sup>†</sup>Wt % of dacite glass in the starting mixture.

Table 4: Compositions and structural formulae (16 O) of experimental plagioclase

Run no.:	PIN87s	PIN88s	PIN89s	PIN97s	PIN98s	PIN98	PIN99	PIN100	PIN102
<i>P</i> (MPa):	400			400		940			960
<i>T</i> (°C):	900			950		750			841
<i>n</i> :	3	4	3	3	3	7	5	10	3
SiO <sub>2</sub>	52.98(67)	55.52(58)	57.63(74)	52.57(33)	56.13(21)	59.05(1.02)	59.72(90)	59.83(1.14)	60.89(34)
Al <sub>2</sub> O <sub>3</sub>	27.99(55)	26.37(98)	25.20(47)	28.04(38)	25.20(35)	23.43(73)	23.89(44)	23.99(85)	24.11(10)
FeO	1.11(40)	0.76(12)	1.16(22)	0.89(3)	1.09(21)	1.88(83)	0.89(60)	1.06(39)	0.55(7)
CaO	11.65(45)	9.71(68)	8.48(41)	12.30(17)	9.86(11)	6.72(28)	6.93(39)	7.04(67)	6.47(23)
Na <sub>2</sub> O	4.31(36)	5.37(34)	5.72(24)	4.03(2)	5.25(4)	6.83(43)	6.96(25)	6.84(32)	7.20(14)
K <sub>2</sub> O	0.20(7)	0.27(6)	0.30(6)	0.12(0)	0.29(3)	0.60(10)	0.45(11)	0.35(6)	0.82(5)
Total	98.23	98.00	98.48	97.97	97.82	99.28	99.17	99.46	100.14
Si	4.91	5.11	5.27	4.88	5.19	5.42	5.41	5.41	5.44
Al	3.06	2.86	2.71	3.07	2.75	2.53	2.55	2.56	2.54
Fe	0.04	0.03	0.04	0.03	0.04	0.06	0.03	0.04	0.02
Ca	1.16	0.96	0.83	1.22	0.98	0.66	0.67	0.68	0.62
Na	0.77	0.96	1.01	0.73	0.94	1.21	1.22	1.20	1.25
K	0.02	0.03	0.03	0.01	0.03	0.07	0.05	0.04	0.09
Ab (mol %)	39.65	49.22	53.95	36.96	48.24	62.46	62.79	62.38	63.63

An (mol %)	59.17	49.15	44.21	62.31	50.00	33.94	34.55	35.51	31.60
Or (mol %)	1.19	1.63	1.84	0.73	1.76	3.60	2.65	2.11	4.77
$K_D^{Ca-Na}$	3.1	2.7	2.7	3.2	2.8	1.4	1.3	1.2	1.5
Run no.:	PIN103	PIN104	PIN105	PIN86	PIN108	PIN87	PIN90	PIN91	PIN94
<i>P</i> (MPa):	960			830	970	830	960		980
<i>T</i> (°C):	841			892	892	892	943		995
<i>n</i> :	5	6	5	9	9	7	4	5	9
SiO <sub>2</sub>	59.03(52)	59.52(96)	56.07(95)	59.66(87)	56.53(56)	57.24(1.01)	59.35(23)	56.00(25)	55.96(87)
Al <sub>2</sub> O <sub>3</sub>	23.95(54)	25.09(99)	27.56(83)	24.41(99)	26.31 (60)	27.16(0.89)	25.60(44)	27.83(28)	27.03(58)
FeO	2.24(43)	0.63(36)	0.46(17)	1.00(34)	0.65(19)	0.60(17)	0.72(4)	0.67(10)	0.85(31)
CaO	7.25(28)	7.84(65)	10.02(73)	7.66(59)	9.25(47)	9.90(49)	8.25(14)	10.43(34)	10.05(23)
Na <sub>2</sub> O	6.81(25)	6.52(29)	5.80(42)	6.32(22)	5.99(25)	5.62(18)	6.40(19)	5.40(15)	5.84(20)
K <sub>2</sub> O	0.45(6)	0.35(10)	0.17(4)	0.45(11)	0.21(5)	0.20(7)	0.34(6)	0.18(3)	0.21(4)
Total	100.45	100.31	100.2	99.93	99.08	100.80	100.74	100.69	100.11
Si	5.37	5.33	5.05	5.38	5.15	5.12	5.29	5.03	5.07
Al	2.57	2.65	2.93	2.59	2.82	2.86	2.69	2.95	2.89
Fe	0.08	0.02	0.02	0.03	0.02	0.02	0.02	0.02	0.03
Ca	0.71	0.75	0.97	0.74	0.90	0.95	0.79	1.00	0.98
Na	1.20	1.13	1.01	1.11	1.06	0.97	1.11	0.94	1.03

K	0.05	0.04	0.02	0.05	0.02	0.02	0.04	0.02	0.02
Ab (mol %)	61.26	58.82	50.66	58.27	53.29	50.06	57.22	47.84	50.63
An (mol %)	36.07	39.08	48.37	38.99	45.48	48.74	40.76	51.10	48.18
Or (mol %)	2.67	2.10	0.97	2.74	1.23	1.20	2.03	1.06	1.19
$K_D^{Ca-Na}$	1.8	1.6	1.9	2.1	1.6	2.1	2.6	3.2	3.0

*n*, number of analyses; numbers in parantheses indicate one standard deviation of replicate analyses in terms of least units cited.

*Table 5: Compositions and structural formulae (23 O) of experimental amphibole*

Run no.:	PIN86s	PIN87s	PIN88s	PIN89s	PIN97s	PIN98	PIN99	PIN100	PIN102	PIN103	PIN104
<i>P</i> (MPa):	400				400	940			960		
<i>T</i> (°C):	900				950	750			841		
<i>n</i> :	5	5	4	4	3	8	10	7	5	3	7
SiO <sub>2</sub>	44.97(86)	45.67(98)	46.62(59)	47.72(67)	44.13(17)	46.17(88)	46.35(83)	46.16(82)	48.44(1.85)	48.75(34)	45.37(49)
Al <sub>2</sub> O <sub>3</sub>	10.59(43)	11.36(19)	9.76(30)	9.31(35)	10.45(24)	11.39(54)	11.69(32)	11.91(1.15)	11.20(79)	10.18(1.73)	12.19(69)
FeO	7.12(1.29)	6.52(17)	7.23(66)	6.31(67)	8.39(44)	8.79(92)	7.13(1.03)	6.08(64)	8.88(1.88)	5.51(38)	10.37(90)
MgO	16.54(68)	15.58(88)	16.74(77)	17.61(41)	16.32(23)	15.45(74)	16.59(64)	17.22(78)	14.53(68)	17.39(1.32)	14.56(88)
MnO	0.26(3)	0.21(13)	0.44(3)	0.00	0.29(6)	0.59(13)	0.47(11)	0.32(7)	0.40(13)	0.30(23)	0.39(9)
CaO	11.78(30)	11.46(37)	11.26(27)	11.40	11.44(4)	11.47(21)	11.48(21)	11.89(21)	10.14(64)	11.64(38)	11.01(42)
Na <sub>2</sub> O	1.93(5)	1.94(14)	1.83(14)	1.72(8)	2.11(5)	1.61(6)	1.56(7)	1.76(7)	2.09(22)	1.87(40)	1.91(11)
K <sub>2</sub> O	0.37(4)	0.41(3)	0.31(3)	0.34(9)	0.32(4)	0.62(11)	0.48(8)	0.44(5)	0.78(25)	0.38(7)	0.43(4)
TiO <sub>2</sub>	0.89(4)	0.99(11)	1.15(12)	1.22(9)	1.44(20)	0.74(10)	0.84(16)	0.83(14)	0.95(17)	1.14(9)	0.95(13)
Total	94.46	94.13	95.34	95.63	94.89	96.83	96.6	96.61	97.40	97.16	97.18
Si	6.65	6.72	6.80	6.88	6.55	6.70	6.67	6.62	7.08	6.97	6.61
Al	1.85	1.97	1.68	1.58	1.83	1.95	1.98	2.01	1.93	1.71	2.09
Fe	0.88	0.80	0.88	0.76	1.04	1.14	0.86	0.72	2.09	1.14	1.39
Mg	3.65	3.43	3.65	3.80	3.62	3.35	3.57	3.69	3.17	3.71	3.17
Mn	0.03	0.03	0.05	0.00	0.04	0.07	0.06	0.04	0.05	0.04	0.05
Ca	1.87	1.81	1.76	1.76	1.82	1.78	1.77	1.83	1.59	1.78	1.72

Na	0.55	0.55	0.52	0.48	0.61	0.45	0.44	0.49	0.58	0.51	0.54
K	0.07	0.08	0.06	0.06	0.06	0.12	0.09	0.08	0.14	0.07	0.08
Ti	0.10	0.11	0.13	0.13	0.16	0.08	0.09	0.09	0.10	0.12	0.10
Mg no.	0.81	0.81	0.81	0.83	0.78	0.75	0.81	0.84	0.60	0.77	0.69
Run no.:	PIN105	PIN106	PIN86	PIN108	PIN87	PIN88	PIN109	PIN110	PIN91	PIN92	
<i>P</i> (MPa):	960		830						960		
<i>T</i> (°C):	841		892						943		
<i>n</i> :	5	5	7	6	6	4	8	8	10	9	
SiO <sub>2</sub>	43.77(66)	44.26(39)	48.26(70)	44.01(38)	45.07(1.56)	44.62(56)	44.05(41)	44.86(54)	44.83(54)	45.56(70)	
Al <sub>2</sub> O <sub>3</sub>	13.40(85)	13.55(31)	10.58(22)	12.60(50)	12.58(37)	12.59(37)	11.81(47)	10.99(29)	12.47(54)	11.22(71)	
FeO	11.03(71)	8.03(66)	7.71(99)	10.26(18)	9.54(1.84)	7.81(61)	9.53(1.02)	8.07(28)	8.45(97)	7.28(52)	
MgO	13.94(43)	15.28(50)	17.34(60)	14.86(48)	15.56(34)	16.46(59)	15.65(53)	16.86(28)	16.34(45)	17.69(48)	
MnO	0.25(5)	0.25(6)	0.38(8)	0.28(10)	0.24(7)	0.20(12)	0.24(9)	0.17(3)	0.26(6)	0.19(8)	
CaO	11.36(40)	11.73(25)	10.92(25)	10.71(24)	11.15(45)	11.78(19)	11.47(41)	11.88(30)	10.94(41)	11.42(36)	
Na <sub>2</sub> O	2.21(9)	2.30(9)	1.74(9)	2.28(14)	2.12(7)	2.29(9)	2.15(11)	2.09(5)	2.28(8)	2.18(14)	
K <sub>2</sub> O	0.43(5)	0.49(5)	0.37(8)	0.38(6)	0.44(11)	0.39(2)	0.44(4)	0.41(5)	0.37(4)	0.39(6)	
TiO <sub>2</sub>	0.83(3)	0.94(5)	0.94(17)	0.95(13)	1.12(26)	1.00(4)	0.95(19)	0.73(8)	1.11(14)	0.84(4)	
Total	97.21	96.82	98.25	96.32	97.83	97.14	96.3	96.06	97.04	96.77	
Si	6.40	6.43	6.84	6.48	6.49	6.43	6.47	6.53	6.48	6.55	

Al	2.31	2.32	1.77	2.19	2.14	2.14	2.04	1.89	2.12	1.90
Fe	1.34	1.09	1.11	1.35	1.19	0.86	1.05	0.76	1.02	0.88
Mg	3.05	3.32	3.67	3.27	3.35	3.54	3.41	3.67	3.53	3.80
Mn	0.03	0.03	0.05	0	0.03	0.02	0	0	0.03	0.02
Ca	1.78	1.83	1.66	1.69	1.72	1.82	1.8	1.85	1.69	1.76
Na	0.63	0.65	0.48	0.65	0.59	0.64	0.61	0.59	0.64	0.61
K	0.08	0.09	0.07	0.07	0.08	0.07	0.08	0.08	0.07	0.07
Ti	0.09	0.10	0.10	0.11	0.12	0.11	0.1	0.08	0.12	0.09
Mg no.	0.69	0.75	0.77	0.71	0.74	0.80	0.76	0.83	0.78	0.81

Run no.:	As10						As11	As12			As26			
<i>P</i> (MPa):	920						920	920			920			
<i>T</i> (°C):	950						950	950			1000			
SiO <sub>2</sub>	50.7	46.8	46.1	45.5	47.3	46.1	44.8	47.42	47.15	45.62	47.86	44.6	44.2	
Al <sub>2</sub> O <sub>3</sub>	12.3	11.7	12.9	12.7	11.5	13.1	12.2	10.74	10.64	11.70	9.76	11.7	12.1	
FeO	4.93	5.69	5.81	6.92	5.74	6.64	6.22	5.53	6.49	5.89	5.56	6.68	6.93	
MgO	16.1	17.5	17	17.8	19.7	16.7	18	17.28	17.16	18.56	18.80	17.8	17.8	
MnO	0.17	0.09	0.16	0.1	0.11	0.14	0.1	0.18	0.11	0.00	0.01	0.05	0.06	
CaO	7.55	9.78	9.91	10.1	8.37	9.47	10.6	10.88	10.72	10.76	10.01	10.5	10.2	
Na <sub>2</sub> O	2.51	2.64	2.67	2.91	2.54	2.96	2.4	2.33	2.17	2.54	2.53	2.63	3.13	
K <sub>2</sub> O	0.7	0.47	0.44	0.47	0.47	0.52	0.38	0.38	0.34	0.48	0.36	0.66	0.57	
TiO <sub>2</sub>	0.59	0.86	0.7	0.56	0.63	0.27	0.66	0.86	0.91	0.48	0.72	0.71	0.62	
Total	95.8	95.8	96.1	97.4	96.7	96.2	95.6	96.44	95.70	96.37	95.71	95.8	95.8	
Si	7.05	6.63	6.52	6.39	6.61	6.52	6.41	6.71	6.70	6.47	6.77	6.39	6.34	
Al	2.02	1.96	2.16	2.11	1.89	2.18	2.05	1.79	1.78	1.95	1.63	1.98	2.04	
Fe	0.57	0.67	0.69	0.81	0.67	0.79	0.74	0.65	0.77	0.70	0.66	0.80	0.83	
Mg	3.33	3.70	3.58	3.72	4.12	3.51	3.83	3.64	3.64	3.92	3.96	3.79	3.80	
Mn	0.02	0.01	0.02	0.01	0.01	0.02	0.01	0.02	0.01	0.00	0.00	0.01	0.01	
Ca	1.13	1.48	1.50	1.52	1.25	1.44	1.62	1.65	1.63	1.63	1.52	1.61	1.57	
Na	0.68	0.72	0.73	0.79	0.69	0.81	0.66	0.64	0.60	0.70	0.69	0.73	0.87	
K	0.12	0.08	0.08	0.08	0.08	0.09	0.07	0.07	0.06	0.09	0.06	0.12	0.10	
Ti	0.06	0.09	0.07	0.06	0.07	0.03	0.07	0.09	0.10	0.05	0.08	0.08	0.07	
Mg no.	0.85	0.85	0.84	0.82	0.86	0.82	0.84	0.85	0.82	0.85	0.86	0.83	0.82	

Run no.:	As26				As27				As28			
<i>P</i> (MPa):	920				920				920			
<i>T</i> (°C):	1000				1000				1000			
SiO <sub>2</sub>	44.2	44.9	43.8	43.7	43.6	44.8	44.1	44	45.6	46	45.1	46.2
Al <sub>2</sub> O <sub>3</sub>	12.2	11.4	12.6	12.2	12.3	11.7	12.1	11.6	11.1	10.5	11.1	11

FeO	6.43	6.41	7.05	7.08	6.81	6.47	6.34	7.87	6.18	4.91	4.59	5.19
MgO	17.6	18.6	18.1	18	17.8	19.9	18	17	18.1	17.8	18.5	18.4
MnO	0.09	0.08	0.18	0.11	0.19	0.08	0.15	0.12	0.13	0.12	0	0
CaO	10.5	10.1	10.7	11	10.9	10.1	10.8	10.8	10.8	11.9	11	11.2
Na <sub>2</sub> O	3.05	3.14	2.64	2.62	2.68	2.48	2.75	2.72	2.71	2.41	2.54	2.7
K <sub>2</sub> O	0.57	0.54	0.49	0.49	0.55	0.49	0.54	0.53	0.56	0.52	0.63	0.61
TiO <sub>2</sub>	0.59	0.51	0.53	0.83	0.58	0.44	0.57	0.95	1.05	0.86	0.8	1.12
Total	95.5	95.8	96.5	96.3	95.6	96.7	95.7	95.8	96.4	95.6	95.3	96.8
Si	6.36	6.42	6.24	6.25	6.27	6.35	6.33	6.33	6.47	6.62	6.49	6.52
Al	2.07	1.92	2.12	2.05	2.08	1.94	2.05	1.96	1.86	1.78	1.88	1.84
Fe	0.77	0.77	0.84	0.85	0.82	0.77	0.76	0.95	0.73	0.29	0.55	0.61
Mg	3.77	3.97	3.85	3.84	3.82	4.20	3.85	3.65	3.83	3.83	3.97	3.87
Mn	0.01	0.01	0.02	0.01	0.02	0.01	0.02	0.01	0.02	0.02	0.00	0.00
Ca	1.62	1.55	1.63	1.69	1.68	1.52	1.66	1.66	1.65	1.84	1.70	1.69
Na	0.85	0.87	0.73	0.73	0.75	0.68	0.76	0.76	0.75	0.67	0.71	0.74
K	0.10	0.10	0.09	0.09	0.10	0.09	0.10	0.10	0.10	0.10	0.11	0.11
Ti	0.06	0.05	0.06	0.09	0.06	0.05	0.06	0.10	0.11	0.09	0.09	0.12
Mg no.	0.83	0.84	0.82	0.82	0.82	0.85	0.83	0.79	0.84	0.93	0.88	0.86

Average compositions except for As10, -11, -12, -26, -27 and -28 for which individual analyses are reported; *n*, number of analyses; numbers in parentheses indicate one standard deviation of replicate analyses in term of least units cited. Mg number =  $Mg/(Mg + Fe_{tot})$ .

Table 6: Compositions and structural formulae (22 O) of experimental phlogopite

Run no.:	As10		
<i>P</i> (MPa):	920		
<i>T</i> (°C):	950		
SiO <sub>2</sub>	44.247	39.083	42.384
Al <sub>2</sub> O <sub>3</sub>	16.835	16.466	14.467
FeO	4.306	4.802	4.917
MgO	18.584	22.042	24.725
MnO	0.05	0.062	0.081
CaO	0.346	0.08	0.158
Na <sub>2</sub> O	1.934	1.628	1.313
K <sub>2</sub> O	6.473	7.591	6.158
TiO <sub>2</sub>	0.515	0.694	0.61
Total	93.57	92.82	94.987
Si	6.2096	5.6648	5.9136
Al	2.7857	2.8140	2.3800
Fe	0.5055	0.5822	0.5738
Mg	3.8874	4.7619	5.1419
Mn	0.0059	0.0076	0.0096
Ca	0.0520	0.0124	0.0236
Na	0.5262	0.4575	0.3552
K	1.1591	1.4039	1.0963
Ti	0.0544	0.0757	0.0640
Mg no.	0.88	0.89	0.90

Mg number = Mg/(Mg + Fe<sub>tot</sub>).



Table 7: Compositions and structural formulae (6 O) of experimental clinopyroxene

Run no.:	PIN98s	PIN99s	PIN108	PIN109	PIN87	PIN88	PIN90	PIN91	PIN92	PIN94	PIN95
<i>P</i> (MPa):	400		970		830		960			980	
<i>T</i> (°C):	950		890		892		943			995	
<i>n</i> :	1	1	6	4	4	3	5	4	4	5	5
SiO <sub>2</sub>	52.11	52.53	48.02(90)	49.55(1.67)	48.41(1.23)	49.89(95)	51.71(1.13)	49.09(53)	48.72(47)	48.83(1.09)	49.92(76)
TiO <sub>2</sub>	0.35	0.12	0.61(11)	0.31(14)	0.73(8)	0.91(19)	0.49(10)	0.60(8)	0.61(7)	0.62(9)	0.48(12)
Al <sub>2</sub> O <sub>3</sub>	5.03	3.19	7.41(1.15)	5.03(1.66)	7.06(90)	8.72(84)	6.55(57)	7.65(1.09)	6.88(25)	7.63(73)	6.01(1.21)
FeO	6.78	6.57	8.31(98)	5.93(1.17)	8.01(0.42)	8.11(28)	7.21(69)	7.90(84)	7.38(45)	9.48(20)	8.28(73)
MgO	14.26	16.03	11.57(79)	13.79(1.05)	12.44(50)	11.50(29)	13.89(89)	13.06(58)	12.96(25)	13.35(1.50)	13.54(94)
MnO	0.59	—	0.30(10)	0.34(12)	0.33(6)	0.27(9)	0.42(6)	0.35(13)	0.21(9)	0.31(15)	0.29(6)
CaO	18.14	17.44	20.61(1.18)	22.70(35)	21.88(0.38)	22.08(28)	18.72(77)	20.33(70)	22.00(34)	18.79(1.54)	20.23(38)
Na <sub>2</sub> O	0.89	0.68	1.10(12)	0.88(12)	0.99(5)	0.98(1)	1.21(17)	1.11(11)	0.94(5)	1.06(14)	1.01(13)
K <sub>2</sub> O	0.20	0.16	0.10(15)	0.02(2)	0.02(2)	0.01(1)	0.13(7)	0.06(2)	0.04(3)	0.02(3)	0.04(7)
Total	98.35	96.71	98.01	98.55	99.88	99.50	100.33	100.15	99.72	100.09	99.80
Si	1.95	1.98	1.81	1.84	1.79	1.74	1.89	1.80	1.80	1.80	1.84
Ti	0.01	0.00	0.02	0.01	0.02	0.03	0.01	0.02	0.02	0.02	0.01
Al <sup>IV</sup>	0.05	0.02	0.19	0.16	0.21	0.26	0.11	0.20	0.20	0.20	0.16
Al <sup>VI</sup>	0.17	0.12	0.14	0.06	0.10	0.13	0.17	0.13	0.10	0.13	0.10

Fe	0.21	0.21	0.26	0.18	0.25	0.25	0.22	0.24	0.23	0.29	0.26
Mg	0.79	0.90	0.65	0.76	0.69	0.64	0.76	0.71	0.71	0.73	0.74
Mn	0.02	0.00	0.01	0.01	0.01	0.01	0.01	0.01	0.01	0.01	0.01
Ca	0.73	0.71	0.83	0.90	0.87	0.88	0.73	0.80	0.87	0.74	0.80
Na	0.06	0.05	0.08	0.06	0.07	0.07	0.09	0.08	0.07	0.08	0.07
K	0.01	0.01	0.00	0.00	0.00	0.00	0.01	0.00	0.00	0.00	0.00
Mg no.	0.79	0.81	0.71	0.81	0.73	0.72	0.77	0.75	0.76	0.72	0.74
En%	45.84	49.70	37.26	41.24	38.08	36.03	44.24	40.68	39.37	41.50	41.38
Fs%	12.23	11.43	15.01	9.95	13.77	14.25	12.89	13.81	12.58	16.53	14.19
Wo%	41.92	38.87	47.73	48.81	48.16	49.71	42.86	45.51	48.05	41.98	44.43

*n*, number of analyses; numbers in parentheses indicate one standard deviation of replicate analyses in term of smallest units cited. Mg number = Mg/(Mg + Fe<sub>tot</sub>).

Table 8: Compositions and structural formulae (6 O) of experimental orthopyroxene

Run no.:	PIN98s	PIN99s	As10		As11		As12				As26		As27		As28		
<i>P</i> (MPa):	400		920		920		920				920		920		920		
<i>T</i> (°C):	950		950		950		950				1000		1000		1000		
<i>n</i> :	1	1	<i>m</i>	<i>m</i>	<i>r</i>	<i>r</i>	<i>m</i>	<i>m</i>	<i>r</i>	<i>r</i>	<i>m</i>	<i>m</i>	<i>m</i>	<i>m</i>	<i>r</i>	<i>r</i>	<i>m</i>
SiO <sub>2</sub>	55.31	55.88	55.31	56.80	54.50	56.57	55.87	56.26	55.71	58.14	56.00	53.69	54.74	54.47	55.46	57.21	53.69
TiO <sub>2</sub>	0.13	0.07	0.07	0.07	0.15	0.02	0.08	0.07	0.07	0.00	0.15	0.07	0.19	0.07	0.13	0.05	0.15
Al <sub>2</sub> O <sub>3</sub>	3.13	2.48	5.19	5.05	3.64	4.43	2.25	2.86	1.80	2.14	2.31	4.88	5.06	3.73	3.22	2.67	4.44
FeO	8.56	7.12	4.49	3.03	8.35	3.24	9.73	3.82	10.41	1.59	7.34	4.20	6.28	5.83	5.19	2.66	6.01
MgO	30.29	29.98	31.74	31.95	32.18	34.09	29.55	34.34	29.81	36.46	30.97	34.06	30.79	32.61	33.80	36.05	33.63
MnO	0.61	—	0.12	0.35	0.26	0.14	0.31	0.24	0.19	0.25	0.28	0.10	0.19	0.13	0.16	0.14	0.05
CaO	1.39	1.27	1.31	0.64	0.72	0.45	0.95	0.50	0.88	0.49	0.99	0.49	0.83	0.65	0.61	0.45	0.43
Na <sub>2</sub> O	0.10	0.14	0.37	0.45	0.08	0.21	0.08	0.02	0.01	0.07	0.15	0.05	0.11	0.07	0.05	0.07	0.05
K <sub>2</sub> O	0.01	0.08	0.23	0.24	0.01	0.14	0.05	0.00	0.00	0.01	0.02	0.04	0.01	0.00	0.02	0.00	0.00
Total	99.54	97.03	98.01	98.55	100.33	100.09	98.87	98.12	98.87	99.15	98.21	97.57	98.20	97.55	98.65	99.31	98.46
Si	1.95	2.01	1.92	1.97	1.90	1.94	1.99	1.96	1.99	1.98	1.99	1.88	1.93	1.92	1.93	1.95	1.87
Ti	0.01	0.01	0.00	0.00	0.00	0.00	0.00	0.00	0.00	0.00	0.00	0.00	0.00	0.00	0.00	0.00	0.00
Al <sup>IV</sup>	0.05	0.00	0.08	0.03	0.10	0.06	0.01	0.04	0.01	0.02	0.01	0.12	0.07	0.08	0.07	0.05	0.13
Al <sup>VI</sup>	0.08	0.13	0.14	0.18	0.04	0.12	0.09	0.08	0.06	0.07	0.08	0.08	0.14	0.08	0.06	0.06	0.05

Fe	0.25	0.21	0.13	0.09	0.24	0.09	0.29	0.11	0.31	0.05	0.22	0.12	0.19	0.17	0.15	0.08	0.18
Mg	1.59	1.61	1.64	1.65	1.67	1.74	1.57	1.78	1.58	1.85	1.64	1.77	1.62	1.72	1.75	1.84	1.75
Mn	0.02	0.00	0.00	0.01	0.01	0.00	0.01	0.01	0.01	0.01	0.01	0.00	0.01	0.00	0.00	0.00	0.00
Ca	0.05	0.05	0.05	0.02	0.03	0.02	0.04	0.02	0.03	0.02	0.04	0.02	0.03	0.02	0.02	0.02	0.02
Na	0.01	0.01	0.03	0.03	0.01	0.01	0.01	0.00	0.00	0.00	0.01	0.00	0.01	0.00	0.00	0.00	0.00
K	0.00	0.01	0.01	0.01	0.00	0.01	0.00	0.00	0.00	0.00	0.00	0.00	0.00	0.00	0.00	0.00	0.00
Mg no.	0.86	0.89	0.93	0.95	0.87	0.95	0.85	0.94	0.84	0.98	0.88	0.94	0.90	0.91	0.92	0.96	0.91
En%	83.92	85.93	90.17	93.67	86.09	94.09	82.78	93.21	82.17	96.71	86.51	92.62	88.19	89.73	90.99	95.19	90.13
Fs%	13.31	11.45	7.16	4.98	12.53	5.02	15.30	5.82	16.09	2.36	11.50	6.41	10.10	9.00	7.83	3.95	9.04
Wo%	2.77	2.62	2.67	1.34	1.38	0.88	1.92	0.97	1.74	0.93	1.99	0.97	1.71	1.28	1.17	0.86	0.82

*m*, metasomatic orthopyroxene (20–40 μm); *r*, rim on original orthopyroxene. Mg number =  $Mg/(Mg + Fe_{tot})$ .

Table 9: Compositions of Fe–Ti oxides and structural formulae (3/4 O)

Run no.:	PIN87s	PIN88s	PIN89s	PIN91s	PIN96s	PIN97s	PIN98s	PIN98	PIN99	PIN100
<i>P</i> (MPa):	400				400			940		
<i>T</i> (°C):	900				950			750		
<i>n</i> :	5	3	2	2	4	1	1	9	6	8
TiO <sub>2</sub>	5.00(56)	5.98(57)	7.11(38)	7.26(4)	9.07(9)	8.99	10.27	8.08(1.59)	7.64(2.03)	5.69(1.72)
Al <sub>2</sub> O <sub>3</sub>	1.76(44)	1.31(7)	1.91(0)	3.06(17)	1.12(9)	1.48	1.12	1.01(13)	1.45(53)	1.49(46)
Fe <sub>2</sub> O <sub>3</sub>	52.24(1.08)	51.39(78)	48.83(75)	42.25(21)	45.79(1.05)	44.77	42.68	49.76(3.28)	49.91(3.86)	53.65(3.32)
FeO	29.61(50)	29.90(28)	30.46(6)	28.56(39)	33.98(56)	34.55	36.09	34.77(1.78)	34.28(1.51)	32.78(1.39)
MgO	2.20(32)	2.75(23)	2.96(16)	3.18(30)	2.03(6)	1.53	1.23	1.35(17)	1.32(8)	1.25(16)
MnO	0.21(21)	—	—	—	0.11(7)	0.07	0.18	0.46(4)	0.58(20)	0.41(16)
Total	91.02	91.33	90.74	84.31(25)	92.09	91.39	91.58	95.43	95.18	95.28
FeO*	76.63(1.40)	76.15(47)	74.40(61)	66.58(21)	75.19(1.49)	75.19(1.49)	74.51	79.55(2.01)	79.20(2.36)	81.06(1.86)
Ti	0.15	0.18	0.22	0.24	0.28	0.28	0.32	0.24	0.23	0.17
Al	0.08	0.06	0.07	0.16	0.05	0.07	0.05	0.05	0.07	0.07
Fe <sup>2+</sup>	1.01	1.02	1.04	1.03	1.15	1.18	1.24	1.14	1.13	1.08
Fe <sup>3+</sup>	1.61	1.57	1.50	1.37	1.39	1.38	1.31	1.47	1.48	1.59
Mg	0.13	0.17	0.18	0.20	0.12	0.09	0.08	0.08	0.08	0.07

Mn	0.01	0.00	0.00	0.00	0.00	0.00	0.01	0.02	0.02	0.01
%U/I	14.99(1.26)	17.20(1.42)	20.57(1.01)	24.20(42)	27.02(45)	28.07	31.96	23.65(4.87)	22.68(5.87)	16.96(5.01)
Run no.:	PIN100	PIN102	PIN103	PIN104	PIN104	PIN105	PIN106	PIN108	PIN109	PIN110
<i>P</i> (MPa):	940	960						970		
<i>T</i> (°C):	750	841						892		
<i>n</i> :	1	7	6	9	1	7	1	10	10	7
TiO <sub>2</sub>	33.56	6.99(1.34)	5.77(1.41)	5.96(1.74)	33.39	5.08(61)	5.37	7.54(20)	6.69(19)	6.63(31)
Al <sub>2</sub> O <sub>3</sub>	1.25	1.81(21)	1.39(6)	1.77(33)	1.63	1.76(23)	1.63	1.84(13)	1.67(9)	1.55(16)
Fe <sub>2</sub> O <sub>3</sub>	31.41	52.42(2.87)	53.49(4.28)	53.21(4.11)	29.06	54.87(94)	53.36	49.87(62)	51.24(56)	51.21(1.46)
FeO	28.70	31.66(1.73)	29.72(1.73)	30.07(1.68)	27.76	26.65(64)	29.32	33.49(52)	32.58(34)	32.29(68)
MgO	0.61	2.75(24)	2.48(21)	2.54(23)	0.77	2.31(29)	2.46	1.98(13)	1.95(8)	2.05(16)
MnO	0.39	0.87(47)	1.26(17)	1.30(11)	0.88	1.29(36)	1.09	28(12)	0.20(10)	0.13(7)
Total	95.92	96.50	94.11	94.85	93.48	94.96	93.23	94.99	94.34	93.85
FeO*	56.97	78.83(2.15)	77.86(3.98)	77.95(2.41)	53.91	79.03(1.23)	77.35	78.37(89)	78.70(65)	78.38(1.94)
Ti	0.668	0.20	0.17	0.18	0.68	0.15	0.16	0.22	0.20	0.20
Al	0.039	0.08	0.07	0.08	0.05	0.08	0.08	0.09	0.08	0.07
Fe <sup>2+</sup>	0.635	1.02	0.98	0.98	0.63	1.62	1.60	1.47	1.52	1.53
Fe <sup>3+</sup>	0.625	1.51	1.59	1.57	0.59	0.97	0.98	1.10	1.08	1.07
Mg	0.024	0.16	0.15	0.15	0.03	0.13	0.15	0.12	0.12	0.12

Mn	0.009	0.03	0.04	0.04	0.02	0.04	0.04	0.01	0.01	0.00
%U/I	65.56	19.23(3.97)	15.93(4.35)	16.58(5.55)	68.82	14.08(1.35)	15.07	22.29(58)	19.76(57)	19.53(87)
Run no.:	PIN86	PIN87	PIN88	PIN90	PIN91	PIN92	PIN94	PIN95	PIN96	
<i>P</i> (MPa):	830			960			980			
<i>T</i> (°C):	892			943			995			
<i>n</i> :	2	4	3	2	4	5	4	5	5	
TiO <sub>2</sub>	6.58(11)	6.10(21)	5.99(17)	7.08(82)	6.25(16)	5.81(11)	6.33(95)	6.21(20)	6.04(56)	
Al <sub>2</sub> O <sub>3</sub>	1.43(7)	1.76(5)	1.86(11)	2.14(7)	2.51(4)	2.06(8)	2.84(7)	2.51(9)	1.91(9)	
Fe <sub>2</sub> O <sub>3</sub>	52.78(31)	53.20(86)	53.10(47)	51.22(1.75)	51.88(40)	53.10(53)	52.34(1.69)	53.07(90)	54.47(1.21)	
FeO	31.65(39)	31.98(37)	32.00(18)	31.46(34)	31.30(45)	30.71(37)	32.54(57)	32.31(22)	31.96(31)	
MgO	2.56(20)	2.15(9)	2.12(4)	3.05(30)	2.68(7)	2.63(7)	2.40(38)	2.34(7)	2.51(12)	
MnO	0.38(13)	0.34(17)	0.20(3)	0.39(14)	0.28(10)	0.38(10)	0.11(10)	0.33(4)	0.28(18)	
Total	95.39	95.53	95.26	95.34	94.90	94.69	96.57	96.77	97.17	
FeO*	79.15(67)	76.86(1.12)	79.79(56)	77.56(1.24)	77.99(58)	78.51(79)	79.65(1.45)	80.08(90)	80.99(1.01)	
Ti	0.19	0.18	0.18	0.21	0.18	0.17	0.18	0.18	0.17	
Al	0.07	0.08	0.09	0.10	0.11	0.09	0.13	0.11	0.09	
Fe <sup>3+</sup>	1.55	1.56	1.56	1.49	1.52	1.56	1.51	1.53	1.57	
Fe <sup>2+</sup>	1.03	1.04	1.05	1.02	1.02	1.00	1.04	1.03	1.02	
Mg	0.15	0.12	0.12	0.18	0.16	0.15	0.14	0.13	0.14	

Mn	0.01	0.01	0.01	0.01	0.01	0.01	0.00	0.01	0.01
%U/I	18.35(14)	17.58(36)	17.46(44)	19.89(2.32)	18.23(54)	16.59(31)	18.75(2.57)	18.06(72)	16.90(1.49)

*n*, number of analyses; numbers in parentheses indicate one standard deviation of replicate analyses in term of smallest units cited; Fe<sup>3+</sup> and Fe<sup>2+</sup> calculated from formula constraints; FeO\* is the total iron analysed with microprobe; U, mol % of ulvÛspinel in the spinel oxide; I, mol % of ilmenite in the rhombohedral oxide, both calculated using the normalization procedure of Stormer (1983).

Table 10: Compositions of experimental glasses (normalized to 100 wt % anhydrous)

Run no.:	PIN86s	PIN87s	PIN88s	PIN89s	PIN91s	PIN96s	PIN97s	PIN98s	PIN99s	PIN98	PIN99	PIN100
$P(\text{MPa})$ :	400					400				940		
$T(^{\circ}\text{C})$ :	900					950				750		
$n$ :	5	6	6	6	2	6	6	6	6	8	9	8
$\text{SiO}_2$	68.8(29)	69.95(39)	72.89(61)	74.52(45)	76.46(35)	66.66(27)	67.52(34)	71.65(54)	74.84(1.76)	73.79(70)	73.54(1.40)	73.25(51)
$\text{Al}_2\text{O}_3$	17.47(17)	16.96(15)	15.36(19)	14.39(25)	13.05(9)	16.89(7)	17.26(18)	15.26(18)	13.62(70)	15.19(89)	15.06(60)	15.76(19)
$\text{FeO}$	1.45(5)	1.35(24)	1.21(20)	0.96(11)	1.17(30)	2.93(20)	2.43(32)	2.08(14)	1.83(25)	1.01(44)	1.31(64)	0.65(11)
$\text{MgO}$	1.21(5)	0.95(8)	0.79(4)	1.08(52)	0.68(18)	2.28(2)	1.63(7)	1(8)	0.66(15)	0.53(57)	0.46(45)	0.57(16)
$\text{CaO}$	4.73(11)	4.06(7)	2.9(20)	2.25(7)	1.99(33)	5.09(10)	4.44(16)	2.99(20)	1.99(33)	2.39(56)	2.80(36)	3.42(13)
$\text{Na}_2\text{O}$	4.27(20)	4.58(25)	4.28(14)	4.02(19)	3.68(6)	4.18(20)	4.71(10)	4.5(17)	4.16(23)	3.42(31)	3.72(35)	3.96(10)
$\text{K}_2\text{O}$	1.66(8)	1.81(7)	2.17(8)	2.38(8)	2.59	1.54(9)	1.63(7)	2.2(8)	2.59(17)	3.43(33)	2.75(13)	2.18(4)
$\text{TiO}_2$	0.31(4)	0.25(11)	0.29(4)	0.28(6)	0.27(16)	0.36(9)	0.3(7)	0.24(5)	0.22(7)	0.18(10)	0.26(29)	0.16(10)
$\text{MnO}$	0.11(8)	0.08(7)	0.11(6)	0.1(7)	0.11(10)	0.06(10)	0.07(7)	0.07(7)	0.1(11)	0.07(6)	0.10(10)	0.05(5)
$\text{H}_2\text{O}^*$	8.99	8.27	7.48	6.73	4.32	8.93	6.59	5.46	4.41	9.04	9.73	10.50
Ab%	52.1	55.7	57.1	57.4	55.3	50.7	55.7	57.8	58.3	47.4	51.1	52.9
An%	33.8	28.9	22.7	18.8	17.5	36.2	30.8	22.5	16.4	19.4	22.6	26.8
Or%	20.0	20.6	25.1	28.6	31.8	20.3	19.4	25.1	30.0	44.8	36.7	29.2

Run no.:	PIN102	PIN103	PIN104	PIN105	PIN106	PIN86	PIN87	PIN88	PIN108	PIN109	PIN110	PIN90
<i>P</i> (MPa):	960					830			970			960
<i>T</i> (°C):	841					892			892			943
<i>n</i> :	3	7	7	7	8	7	8	9	8	8	8	8
SiO <sub>2</sub>	73.48(1.71)	75.53(66)	74.26(44)	72.13(53)	70.96(55)	75.03(1.08)	71.34(1.19)	69.67(1.52)	71.96(85)	70.00(34)	70.23(63)	73.48(45)
Al <sub>2</sub> O <sub>3</sub>	15.47(1.81)	14.37(54)	15.48(25)	17.01(26)	17.66(18)	14.39(15)	16.65(21)	17.58(20)	16.41(28)	17.70(21)	17.76(15)	14.72(16)
FeO	0.68(30)	0.75(21)	0.74(22)	0.69(11)	0.81(31)	0.89(12)	0.95(11)	1.06(13)	1.12(44)	1.22(15)	1.29(15)	0.98(12)
MgO	0.46(34)	0.39(9)	0.44(3)	0.28(6)	0.31(3)	0.52(8)	0.57(6)	0.54(14)	0.58(9)	0.75(13)	0.46(6)	0.89(7)
CaO	2.19(87)	2.24(18)	2.80(15)	3.70(22)	4.14(26)	2.30(6)	3.68(23)	4.11(16)	3.13(11)	4.12(15)	4.40(17)	2.35(17)
Na <sub>2</sub> O	3.68(1.11)	3.73(26)	3.76(17)	4.01(33)	4.11(11)	4.00(11)	4.41(16)	4.99(11)	3.29(7)	4.17(16)	3.93(19)	4.74(8)
K <sub>2</sub> O	3.82(57)	2.74(8)	2.28(5)	1.86(6)	1.72(9)	2.61(16)	2.07(6)	1.76(3)	2.12(12)	1.67(6)	1.63(12)	2.47(5)
TiO <sub>2</sub>	0.19(8)	0.20(5)	0.20(7)	0.25(8)	0.26(4)	0.20(5)	0.21(7)	0.23(6)	0.27(7)	0.26(5)	0.24(6)	0.25(4)
MnO	0.03(5)	0.05(4)	0.04(4)	0.06(9)	0.03(4)	0.06(5)	0.12(11)	0.04(6)	0.11(7)	0.11(7)	0.06(7)	0.12(8)
H <sub>2</sub> O*	7.16	7.98	9.54	10.34	11.69	6.35	7.96	9.32	8.15	10.40	12.91	5.96
Ab%	48.2	53.6	53.8	53.61	53.12	55.77	55.05	57.79	56.42	53.81	51.38	60.42
An%	16.8	18.9	23.5	29.04	31.39	18.83	26.89	27.95	24.10	31.15	33.77	17.57
Or%	44.6	35.5	31.0	25.10	23.42	32.72	25.89	21.35	27.18	23.16	23.73	27.92

Run no.:	PIN91	PIN92	PIN94	PIN95	PIN96	As10	As11	As12	As26	As27	As28
<i>P</i> (MPa):	960		980			920			920		

<i>T</i> (°C):	943		995			950			1000			
<i>n</i> :	8	8	7	8	9	12	11	10	6	10	6	
SiO <sub>2</sub>	70.20(54)	68.96(48)	69.63(50)	67.82(66)	67.37(92)	71.19 (42)	70.41(36)	71.06 (65)	69.20(52)	70.00 (87)	69.47 (70)	
Al <sub>2</sub> O <sub>3</sub>	16.83(27)	17.41(21)	17.04(25)	17.09(20)	16.83(25)	19.03 (31)	19.00 (17)	18.74 (15)	20.78(34)	20.14 (27)	20.28 (17)	
FeO	1.16(15)	1.43(19)	1.49(14)	1.83(23)	2.14(22)	1.16 (18)	1.47 (08)	1.35 (16)	1.21(20)	1.80 (24)	1.65 (24)	
MgO	0.97(14)	1.02(10)	0.89(22)	1.55(21)	1.48(65)	0.36 (17)	0.67 (25)	0.49 (14)	0.24(19)	0.23 (6)	0.26 (0.06)	
CaO	3.27(12)	4.03(17)	3.07(8)	4.10(22)	5.13(17)	2.22 (15)	2.69 (10)	2.46 (15)	2.44(22)	3.56 (42)	2.87 (24)	
Na <sub>2</sub> O	5.42(18)	5.27(9)	5.41(17)	5.53(16)	5.13(12)	3.75 (27)	3.48 (19)	3.46 (15)	4.43(39)	2.39 (25)	3.44 (24)	
K <sub>2</sub> O	1.83(6)	1.56(4)	2.01(13)	1.67(9)	1.46(12)	1.80 (05)	1.83 (08)	1.91 (08)	1.14(11)	1.34 (10)	1.37 (18)	
TiO <sub>2</sub>	0.24(5)	0.26(6)	0.33(7)	0.32(5)	0.36(9)	0.08 (03)	0.14 (05)	0.12 (04)	0.10(5)	0.18 (5)	0.14 (4)	
MnO	0.08(7)	0.07(8)	0.13(7)	0.10(8)	0.10(10)	0.04 (03)	0.04 (04)	0.05 (06)	0.04(3)	0.04 (3)	0.03 (2)	
H <sub>2</sub> O*	6.81	8.52	4.79	5.31	7.56	11.92	11.44	11.75	12.61	13.58	13.02	
Ab%	62.94	60.42	62.79	60.77	56.06	57.47	56.82	53.61	54.43	51.04	52.23	
An%	22.25	27.09	20.91	26.45	32.82	15.15	12.77	8.21	16.91	13.53	17.00	
Or%	20.19	18.33	22.06	18.75	17.74	31.48	34.39	41.25	33.50	40.19	36.04	

\* H<sub>2</sub>O determined by using the by-difference method (see text).

Table 11: Representative compositions and structural formulae (23 O) of natural amphiboles of Pinatubo dacite

low Al <sub>2</sub> O <sub>3</sub> amphibole															
SiO <sub>2</sub>	46.43	46.63	48.41	48.35	46.07	44.64	48.29	46.06	47.60	47.11	47.76	47.15	48.15	48.32	46.33
Al <sub>2</sub> O <sub>3</sub>	8.18	8.02	6.96	6.84	8.88	9.03	7.46	7.81	7.75	8.35	7.50	6.85	6.34	7.08	8.33
FeO	13.81	13.60	12.66	12.96	13.98	13.25	13.04	13.08	13.26	13.69	12.41	12.15	12.17	13.07	12.80
MgO	14.21	14.28	15.47	15.55	14.23	14.41	15.68	14.85	14.85	14.43	15.83	16.13	16.25	15.87	14.33
MnO	0.58	0.41	0.53	0.66	0.26	0.54	0.45	0.70	0.45	0.56	0.28	0.34	0.43	0.29	0.41
CaO	11.15	11.23	10.78	10.90	10.70	10.56	10.34	11.40	10.76	10.53	10.68	10.75	10.67	10.43	10.48
Na <sub>2</sub> O	1.32	1.27	1.20	1.30	1.67	1.61	1.22	1.22	1.32	1.47	1.36	1.24	1.09	1.26	1.35
K <sub>2</sub> O	0.30	0.28	0.25	0.20	0.23	0.31	0.30	0.36	0.32	0.33	0.26	0.18	0.13	0.25	0.38
TiO <sub>2</sub>	0.77	0.87	0.90	0.75	1.32	1.19	0.91	0.87	0.96	1.06	1.29	0.89	1.02	0.98	1.13
Total	96.75	96.58	97.16	97.51	97.35	95.54	97.68	96.34	97.26	97.52	97.38	95.68	96.24	97.54	95.54
Si	6.72	6.75	6.89	6.86	6.61	6.51	6.79	6.68	6.80	6.72	6.76	6.78	6.87	6.81	6.74
Al	1.39	1.37	1.17	1.14	1.50	1.55	1.24	1.34	1.30	1.40	1.25	1.16	1.07	1.18	1.43
Fe	1.67	1.65	1.51	1.54	1.68	1.62	1.53	1.59	1.58	1.63	1.47	1.46	1.45	1.54	1.56
Mg	3.06	3.08	3.28	3.29	3.04	3.13	3.29	3.21	3.16	3.07	3.34	3.46	3.45	3.33	3.11
Mn	0.07	0.05	0.06	0.08	0.03	0.07	0.05	0.09	0.05	0.07	0.03	0.04	0.05	0.03	0.05
Ti	0.08	0.09	0.10	0.08	0.14	0.13	0.10	0.10	0.10	0.11	0.14	0.10	0.11	0.10	0.12
Ca	1.73	1.74	1.64	1.66	1.64	1.65	1.56	1.77	1.65	1.61	1.62	1.66	1.63	1.57	1.63
Na	0.37	0.36	0.33	0.36	0.47	0.46	0.33	0.34	0.36	0.41	0.37	0.35	0.30	0.35	0.38
K	0.05	0.05	0.05	0.04	0.04	0.06	0.05	0.07	0.06	0.06	0.05	0.03	0.02	0.04	0.07
Mg no.	0.65	0.65	0.69	0.68	0.64	0.66	0.68	0.67	0.67	0.65	0.69	0.70	0.70	0.68	0.67

low Al <sub>2</sub> O <sub>3</sub> amphibole	high Al <sub>2</sub> O <sub>3</sub> amphibole													
SiO <sub>2</sub>	46.18	46.48	44.92	41.52	41.85	42.82	41.73	41.31	41.78	41.43	41.07	43.31	42.16	44.62
Al <sub>2</sub> O <sub>3</sub>	7.80	7.89	8.81	12.55	11.36	11.63	12.22	12.57	11.85	11.89	11.19	10.49	10.71	10.52
FeO	13.82	13.04	13.79	14.37	10.74	13.11	9.56	8.91	10.10	9.10	11.93	12.10	11.97	14.70
MgO	14.48	14.48	14.13	12.25	15.16	13.61	15.48	15.42	15.14	15.84	13.80	14.62	14.11	13.04
MnO	0.46	0.61	0.57	0.25	0.16	0.38	0.08	0.00	0.15	0.10	0.31	0.31	0.27	0.47
CaO	10.53	10.45	11.04	11.29	11.60	11.12	12.02	12.17	11.92	11.72	11.45	11.15	11.59	10.55
Na <sub>2</sub> O	1.22	1.23	1.51	2.14	2.00	1.83	2.13	2.12	2.05	2.09	1.87	1.88	1.85	1.72
K <sub>2</sub> O	0.28	0.32	0.38	0.33	0.44	0.41	0.52	0.52	0.48	0.54	0.50	0.44	0.50	0.49

TiO <sub>2</sub>	0.99	0.95	1.11	2.08	2.15	2.05	2.23	2.17	2.19	2.24	2.12	2.13	2.08	1.26
Total	95.76	95.45	96.23	96.78	95.45	96.96	95.97	95.19	95.66	94.94	94.23	96.43	95.23	97.37
Si	6.70	6.75	6.55	6.11	6.14	6.21	6.10	6.09	6.14	6.09	6.16	6.29	6.26	6.44
Al	1.33	1.35	1.51	2.18	1.96	1.99	2.11	2.18	2.05	2.06	1.98	1.80	1.87	1.79
Fe	1.68	1.58	1.68	1.77	1.32	1.59	1.17	1.10	1.24	1.12	1.50	1.47	1.49	1.77
Mg	3.13	3.13	3.07	2.69	3.32	2.94	3.37	3.39	3.31	3.47	3.09	3.17	3.12	2.80
Mn	0.06	0.08	0.07	0.03	0.02	0.05	0.01	0.00	0.02	0.01	0.04	0.04	0.03	0.06
Ti	0.11	0.10	0.12	0.23	0.24	0.22	0.24	0.24	0.24	0.25	0.24	0.23	0.23	0.14
Ca	1.64	1.63	1.72	1.78	1.82	1.73	1.88	1.92	1.88	1.85	1.84	1.74	1.84	1.63
Na	0.34	0.35	0.43	0.61	0.57	0.52	0.60	0.61	0.58	0.59	0.54	0.53	0.53	0.48
K	0.05	0.06	0.07	0.06	0.08	0.08	0.10	0.10	0.09	0.10	0.10	0.08	0.09	0.09
Mg no.	0.65	0.66	0.65	0.60	0.72	0.65	0.74	0.76	0.73	0.76	0.67	0.68	0.68	0.61

Microprobe analyses were performed on several phenocryst grains, hand picked from a gently crushed pumice. Several grains were mounted in epoxy resin and analysed with analytical conditions similar to those for experimental run products (see text). All analyses are from the apparent core of the phenocrysts. Mg number =  $Mg/(Mg + Fe_{tot})$ .

Table 12: Comparison between the Pinatubo dacite and selected melts from dehydration or fluid-present melting of basalts in the pressure range 2000–3800 MPa and interactions of these with peridotite

	Pinatubo	RW-95	RW-95	RW-95	SD-94	SD-94	WN-91	P-01	P-01	R <i>et al.</i>	P-01
Nature:		melting	melting	melting	melting	melting	melting	melting	melting	interaction	interaction
Dehydration:		yes	yes	yes	yes	yes	—	—	—	—	—
Fluid present:		—	—	—	—	—	yes	yes	yes	—	—
<i>P</i> (MPa):	—	2200	2200	3200	2000	2000	2970	3000	3000	3800	1500
<i>T</i> (°C):	—	1025	1050	1100	975	950	900	900	1000	1100	900
SiO <sub>2</sub>	64.6	66.0	65.9	65.93	66.18	67.66	74.9	70.9	68.0	65.43	64.2
TiO <sub>2</sub>	0.53	0.61	0.81	1.31	0.78	0.61	0.41	0.30	0.30	1.98	0.5
Al <sub>2</sub> O <sub>3</sub>	16.5	18.24	17.83	17.55	17.81	17.45	13.9	16.1	17.9	12.91	18.8
FeO	4.37	3.29	3.40	3.15	2.48	1.89	1.28	0.5	1.2	4.05	1.1
MgO	2.39	0.89	1.17	1.02	0.68	0.62	0.21	0.1	0.2	2.75	1.5
CaO	5.23	4.17	4.70	1.47	1.88	1.61	1.47	1.4	1.1	2.15	1.0
Na <sub>2</sub> O	4.49	6.26	5.40	6.72	5.70	4.89	4.95	9.3	7.1	6.25	11.4
K <sub>2</sub> O	1.54	0.52	0.49	2.55	4.50	5.29	2.87	1.5	1.1	3.83	1.5
H <sub>2</sub> O	>10										

RW-95, Rapp & Watson (1995); SD-94, Sen & Dunn (1994a); WN-91, Winther & Newton (1991); P-01, Prouteau *et al.* (2001); R *et al.*, Rapp *et al.* (1999). The nature of experiment denotes either melting under fluid-absent or fluid-present condition, or slab melt–peridotite interaction.

